International Journal of Coal Geology 267 (2023) 104182

Contents lists available at ScienceDirect

International Journal of Coal Geology

journal homepage: www.elsevier.com/locate/coal

Carbon isotopic composition and organic petrography of thermally metamorphosed Antarctic coal: Implications for evaluation of $\delta^{13}C_{org}$ excursions in paleo-atmospheric reconstruction

Margaret M. Sanders [a], Susan M. Rimmer [a,*], Harold D. Rowe [b]

[a] School of Earth Systems and Sustainability, Southern Illinois University Carbondale, Carbondale, IL 62901, USA
[b] Premier Oilfield Laboratories, 11335 Clay Rd., Houston, TX 77041, USA

ARTICLE INFO

Keywords:
Stable carbon isotopes
Organic maturation
Natural cokes
Pyrolytic carbon
Contact metamorphism

ABSTRACT

Large, globally documented negative $\delta^{13}C$ excursions that occur across the Permian-Triassic transition are thought to represent the isotopic fingerprint of considerable releases of isotopically light carbon into the atmosphere, with the largest of these excursions (as much as −22.2‰) measured in bulk organic matter in coals and carbonaceous shales from Antarctica. Previous studies have attributed the carbon isotopic excursion (CIE) at the Permian–Triassic boundary to the release of CH_4 from organic-rich rocks intruded by dikes and sills associated with the Siberian Traps flood basalts (Russia) and Longwood-Bluff (New Zealand) intrusions. However, any assessment of paleoatmospheric conditions based on this or other $\delta^{13}C_{org}$ excursions must consider the multiple controls on isotopic composition, including maceral content and post-depositional diagenetic and maturation processes. Permian-age coal seams and associated sediments in Antarctica were extensively altered after burial by localized high heat flow and, in some cases, by contact metamorphism associated with Jurassic dikes and sills. Levels of organic maturation reach anthracite, meta-anthracite, and even graphite; such intense thermal alteration had the potential to change the carbon isotopic composition of the bulk organic matter ($\delta^{13}C_{org}$). To evaluate the Permian–Triassic isotopic excursion in Antarctica, it is important to understand the inherent variability in $\delta^{13}C_{org}$ in Permian-age coal and organic-rich sedimentary rocks prior to the CIE; thus, 128 samples representing pre-boundary coals and shales were selected from the United States Polar Rock Repository for analysis. Petrographic (maceral analysis and vitrinite reflectance), geochemical (C, H, N), and carbon isotopic analyses were performed. Based on the presence of coarse-grained circular and fine-grained lenticular mosaic in the anisotropic cokes found in samples in close proximity to intrusions, the rank of the samples prior to intrusion is estimated to have been medium volatile bituminous (~1.2% R_{max}). These highly altered coals and cokes can have random vitrinite reflectances (R_r) exceeding 6%. Subsequent to intrusion, alteration beyond the contact aureoles continued due to high heat flow, producing high rank coals with $R_r > 2\%$. Values of $\delta^{13}C_{org}$ range between −26.5 and −21.1‰ (5.4‰ difference). Significant relationships (at the 1 and 5% levels) exist between $\delta^{13}C_{org}$ and the level of organic maturity, organic carbon (C_{org}) content (i.e., size of the carbon reservoir), and total inertinite content, suggesting variability due to these factors should be considered when assessing isotopic excursions and interpretation of Permian-Triassic atmospheric conditions. These findings highlight the importance of incorporating organic petrography into $\delta^{13}C_{org}$ studies.

1. Introduction

Numerous studies have focused on the cause(s) of the mass extinction event at the Permian–Triassic boundary. The changes in global atmospheric and oceanic conditions are thought to have been catastrophic, resulting in a substantial loss of marine and terrestrial life (Raup and Sepkoski, 1982; Retallack, 1995; Hallam and Wignall, 1997; Retallack and Krull, 1999; de Wit et al., 2002; Erwin, 2006; Shen et al., 2011; Stanley, 2016). Large negative stable carbon isotope excursions (CIEs) occur across the boundary, indicating a considerable release of isotopically light carbon into the atmosphere (Faure et al., 1995; Holser et al., 1996; Kump and Arthur, 1999; Wignall, 2001; Berner, 2002;

* Corresponding author.
E-mail address: srimmer@siu.edu (S.M. Rimmer).

https://doi.org/10.1016/j.coal.2022.104182
Received 26 September 2022; Received in revised form 23 December 2022; Accepted 30 December 2022
Available online 5 January 2023

Retallack and Jahren, 2008; Svensen et al., 2009; Shen et al., 2012; Polozov et al., 2016; Wu et al., 2021). These excursions are evident worldwide in the carbon isotope values of carbonate, bone, and organic matter (OM) (Retallack et al., 2006). Various $\delta^{13}C_{org}$ excursions in terrestrial sections have been recognized in South China (Shen et al., 2011; Wu et al., 2021), Antarctica (Krull et al., 2000), Australia (Morante, 1996), Germany (Scholze et al., 2017), and Pakistan (Schneebeli-Hermann et al., 2013). de Wit et al. (2002) report large negative $\delta^{13}C_{org}$ excursions, with terrestrial OM becoming more depleted by as much as 5–15‰ at the Permian–Triassic boundary in five major Gondwanan basins in India, Madagascar, and South Africa. Similar negative excursions were documented globally in marine carbonates (Magaritz et al., 1988; Baud et al., 1989; Holser et al., 1989; Xu and Yan, 1993; Yin et al., 1996; Jin et al., 2000; de Wit et al., 2002; Richoz, 2006; Horacek et al., 2007a, 2007b; Korte and Kozur, 2010; Shen et al., 2013; Schobben et al., 2016; Bagherpour et al., 2020; Saitoh and Isozaki, 2021) and C_{org} from marine strata (Morante, 1996; Wignall et al., 1998; Twitchett et al., 2001; Cao et al., 2002; Grasby and Beauchamp, 2008; Takahashi et al., 2010; Algeo et al., 2012; Zuchuat et al., 2020).

Hypotheses on the cause of the excursions suggest the release of isotopically light gases such as CH_4 or CO_2 into the atmosphere, including CH_4 from deep-ocean water overturn or shoaling of deep-water (Kajiwara et al., 1994; Knoll et al., 1996; Ryskin, 2003; Algeo et al., 2007), increased microbial methanogenesis (Rothman et al., 2014), volcanogenic CO_2 emission (Renne et al., 1995; Hansen, 2006), methane clathrate outbursts (Erwin, 1993; Morante, 1996; Krull et al., 2000, 2004; Brand et al., 2016), igneous intrusions into organic-rich rocks (Krull et al., 2000, 2004; Berner, 2002; Sarkar et al., 2003; Retallack and Jahren, 2008; Ganino and Arndt, 2009; Grasby et al., 2011; Shen et al., 2012; Rampino et al., 2017), both volcanic CO_2 emission and CH_4 generation associated with intrusions (Wu et al., 2021), and oxidation of sedimentary OM (Baud et al., 1989; Holser et al., 1989; Ward et al., 2000; Sephton et al., 2005). The timing of the massive Siberian Traps (Russia) and Longwood-Bluff (New Zealand) eruptions that intruded coal basins (Czamanske et al., 1998) may have resulted in significant release of gases coinciding with the Permian-Triassic extinction (Renne and Basu, 1991; Campbell et al., 1992; Kamo et al., 2003; Reichow et al., 2009; Burgess and Bowring, 2015). Whereas the timing of these eruptions suggests a correlation, a much larger mass of mantle CO_2 with a $\delta^{13}C$ value of −7‰ to −5‰ (Dickens et al., 1995), which is isotopically heavier than CH_4, would have to degas to create the observed spikes (Berner, 2002). However, if the coupled processes of contact metamorphism of organic-rich sediments and the generation of CH_4 are included, this explanation becomes more viable (McElwain et al., 2005; Retallack and Greaver, 2007).

Some of the largest excursions, up to −22.2‰, have been measured in sedimentary rocks from Antarctica (Retallack and Jahren, 2008). Using carbon isotope chemostratigraphy, they found that the negative excursions in Antarctica were coincident with the large climate shift across the Permian–Triassic boundary. Retallack and Jahren (2008) attribute the large $\delta^{13}C$ excursions at the Permian–Triassic boundary to the release of large amounts of CH_4 from organic-rich rocks intruded by igneous rocks at that time. This same mechanism was proposed by Svensen et al. (2004, 2007) to explain the $\delta^{13}C_{org}$ excursions during the Paleocene–Eocene Thermal Maximum (PETM) and the Toarcian oceanic anoxic event (T-OAE).

Because Antarctic coal is known to be heavily intruded and highly metamorphosed by Jurassic dikes and sills associated with the Karoo-Ferrar Large Igneous Province (LIP) (Schopf and Long, 1966; Coates et al., 1990; Elliot et al., 1999; Faure and Mensing, 2010; Sanders and Rimmer, 2020), the $\delta^{13}C_{org}$ values may not accurately reflect the $\delta^{13}C$ values of the Permian atmosphere due to significant changes during organic maturation. To date, there have been no studies of $\delta^{13}C_{org}$ for Antarctic coals and other organic-rich rocks that have considered thermal alteration of OM, weathering, variations in maceral composition, release of coal-bed CH_4, size of the C_{org} reservoir, or possible trapping of volatiles as pyrolytic carbon within the seams, and how these factors may contribute to the isotopic variability. Any assessment of the excursions in carbon isotopic composition that are used to infer global atmospheric composition and climate change at the Permian–Triassic boundary (or others associated with CIEs) should consider the natural variability in and influences on $\delta^{13}C_{org}$. Thus, the objectives of this study were to analyze Late Permian organic-rich samples (i.e., prior to the CIE at the boundary) from various locations along the Transantarctic Mountains (TAM) in order to 1) determine the natural range in $\delta^{13}C_{org}$ for Antarctic coals and carbonaceous shales, 2) assess possible controls on $\delta^{13}C_{org}$ in these samples, including such factors as maceral composition and level of thermal maturation, and 3) highlight the factors that should be considered when organic-rich Antarctic samples are used to assess Permian–Triassic boundary excursions.

1.1. Geologic setting

Most known Antarctic coal lies in the exposed strata of the fault-block TAM that span the continent (Schapiro and Gray, 1966). The present study includes coal and organic-rich sedimentary rocks from several Permian coal-bearing formations in the TAM, including the Mt. Glossopteris, Queen Maud, and Buckley formations, and the Weller Coal Measures (Figs. 1 and 2). The Mt. Glossopteris Formation is thought to be Late Permian in age (~270 to 250 Ma) and time correlative with all of the coal and sandstone-shale sequences sampled for this study (Long, 1965; Collinson et al., 2006; Faure and Mensing, 2010). These formations are part of the Beacon Supergroup that, in addition to the Ferrar Dolerite and Kirkpatrick Basalt, compose the majority of the mountain range (Barrett et al., 1986; Faure and Mensing, 2010) (Fig. 2). The Mt. Glossopteris Formation consists of cyclical deposits of arkose, feldspathic sandstone, siltstone, shale, and coal. Located in the Ohio Range, where it is capped by a thick diabase sill of the Ferrar Dolerite, the coal and carbonaceous shale layers include *Glossopteris* and *Gangamopteris* leaves (Long, 1962, 1965; Schopf, 1962; Cridland, 1963; Faure and Mensing, 2010). Individual coal beds in the Mt. Glossopteris Formation range in thickness from 1.2 to 3.6 m, with a total thickness of around 23 m (Schopf, 1962; Schopf and Long, 1966; Faure and Mensing, 2010). The Queen Maud Formation, which also contains *Glossopteris* fossils, is located at Mt. Weaver and is lithologically similar to the Mt. Glossopteris Formation (Minshew, 1966). The Buckley Formation and its equivalents appear to contain the most extensive of the coal measures, with exposures ranging from the Byrd Glacier to the Amundsen Glacier (Nilsen Plateau). The formation is primarily sandstone with carbonaceous shale and coal beds that contain various plant fossils (Barret, 1969; Barrett et al., 1986; Faure and Mensing, 2010). The seams are generally 1–2 m thick, similar to the Mt. Glossopteris Formation, with the thickest (10.7 m) located on Mount Picciotto in the Queen Elizabeth Range (Barrett et al., 1986). Located in southern Victoria Land, the Weller Coal Measures are comprised of carbonaceous sandstone and siltstones that include both *Glossopteris* and *Gangamopteris* leaves (Faure and Mensing, 2010).

During the Early Jurassic (Toarcian) (176–177 Ma), flood basalts and diabase sills and dikes of the Ferrar Group intruded the sedimentary rocks of the Beacon Supergroup (Fleming et al., 1997; Faure and Mensing, 2010). These intrusions were associated with the Karoo–Ferrar LIP (Pálfy and Smith, 2000), one of the most voluminous LIPs to form during the Phanerozic (Rampino and Strothers, 1988); this may have been related to crustal rifts during the break-up of Gondwana, however the association of the two events has been debated (Faure and Mensing, 2010; Broger, 2011). A belt of similar eruptions extends across southern Africa, India, South America, and Australia (Faure, 2001). Numerous sills (some dozens of meters thick) intrude the Beacon Supergroup in the TAM; in one area of the Queen Alexandra Range, five sills intrude the supergroup and potentially more are unexposed (Faure and Mensing, 2010). The massive sills have affected the topography by uplifting areas of the mountain range and protecting underlying sedimentary rocks

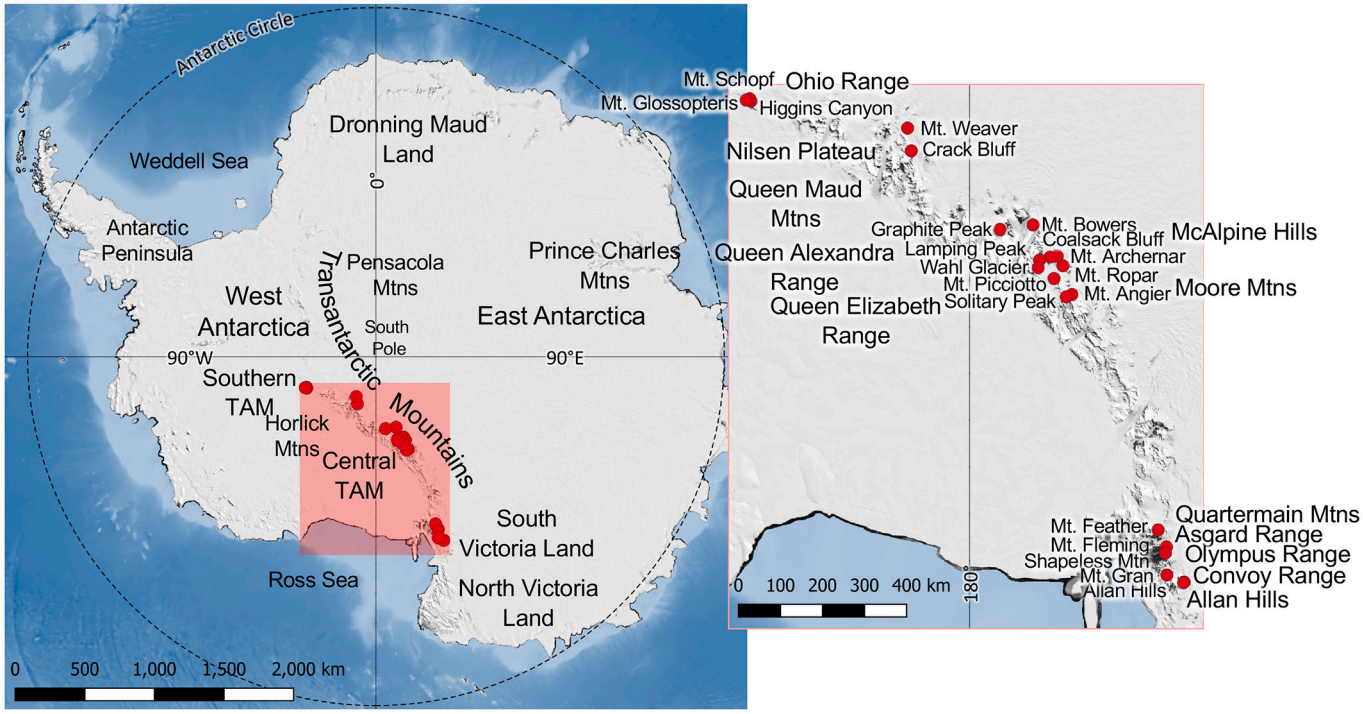

Fig. 1. Map showing sample locations along the Transantarctic Mountain Range (TAM). Base map source: Quantarctica, Norwegian Polar Institute (Matsuoka et al., 2018, 2021). Mtns = Mountains, Mt. = Mount. (Modified from Sanders and Rimmer, 2020).

from erosion (Faure and Mensing, 2010). Contact metamorphism was documented in the sandstones, shale, and coal of the Beacon Supergroup (Faure and Mensing, 2010), and examples exist of contact aureoles affecting the coal measures (e.g., Schapiro and Gray, 1966; Sanders and Rimmer, 2020).

The current rank of many Antarctic coals is higher than any comparable Gondwanan coal due to the extensive Jurassic intrusions (Schopf and Long, 1966; Coates et al., 1990; Sanders and Rimmer, 2020). Widespread diabase sills have caused varying degrees of thermal alteration (Schapiro and Gray, 1966; Schopf and Long, 1966; Coates et al., 1990; Sanders, 2012; Sanders and Rimmer, 2020). Many of the samples are anthracite, meta-anthracite, or natural coke, indicating very high levels of maturation (Schopf and Long, 1966; Sanders and Rimmer, 2020). Based on petrographic analyses, some samples are so highly metamorphosed that they are approaching graphite (Schapiro and Gray, 1966; Sanders, 2012). Despite considerable petrographic and geochemical studies of Antarctic coals (e.g., Schapiro and Gray, 1966; Schopf and Long, 1966; Coates et al., 1990; Sanders and Rimmer, 2020), no previous work has attempted to relate isotopic composition to factors such as coal rank and maceral composition for these coals.

2. Methods

2.1. Sampling

Samples used in this study were part of a larger petrographic and geochemical effort (proximate, ultimate, and total sulfur) to understand the occurrence, composition, and thermal alteration history of Antarctic coals (Sanders, 2012; Sanders and Rimmer, 2020). These included coal and carbonaceous shale samples stored at the Polar Rock Repository (PRR) at The Ohio State University, which is sponsored by the National Science Foundation Office of Polar Programs. Details of the sampling are available in appendices and tables in Sanders and Rimmer (2020). In brief, these include 128 samples of Permian coal or organic-rich shale collected at various locations in the TAM during past expeditions including the Southern Transantarctic Mountains, the Central Transantarctic Mountains, and South Victoria Land (Fig. 1). Due to the difficulty in sampling and field conditions, these samples are characterized as "grab" samples. All are Permian in age, and include 64 samples from the Buckley Formation, 22 from the Mt. Glossopteris Formation, 23 from the Queen Maud Formation, and 19 from the Weller Coal Measures.

2.2. Organic petrography

Samples were crushed to minus 20-mesh and petrographic pellets were prepared according to standard procedures, ground, and polished to a final polish of 0.06-μm. Point-count analyses (500 points on each of two pellets) were performed on a subset of samples (34), randomly selected from each location, using a Zeiss Universal reflected-light microscope equipped with crossed polarizers and an antiflex objective that includes a 1/4λ plate to enhance anisotropy. Point-count categories included vitrinite, anisotropic coke, inertinite, semi-inertinite (i.e., inertinite with lower reflectance, typically with reflectance levels ~ < 2% as suggested by ASTM D2799–13 (ASTM, 2013)), and pyrolytic carbon (Table 1). Photomicrographs were taken using a Q-Imaging Retiga 2000R camera.

Random vitrinite reflectance (100 readings per sample) (R_r, % in oil) was determined for a subset of samples (91) following standard procedures (ASTM, 2011) using a Leica DM2500P reflected-light microscope (non-polarized light) and J&M MSP200 hardware and software (Table 1). The system was calibrated with three standards, with a typical standard deviation of 0.02%. Standards used for samples <6% R_r included glass (1.672%), cubic zirconia (3.17%), and strontium titanate (5.46%); for samples >6% R_r, cubic zirconia, strontium titanate, and silicon carbide (7.45%) were used. Mean maximum reflectance (R_{max}, % in oil) was also measured using polarized light for randomly selected pellets from each location (13 samples) using the J&M MSP200 system (Table 1). All petrography was performed at the Organic Petrology Laboratory at Southern Illinois University Carbondale.

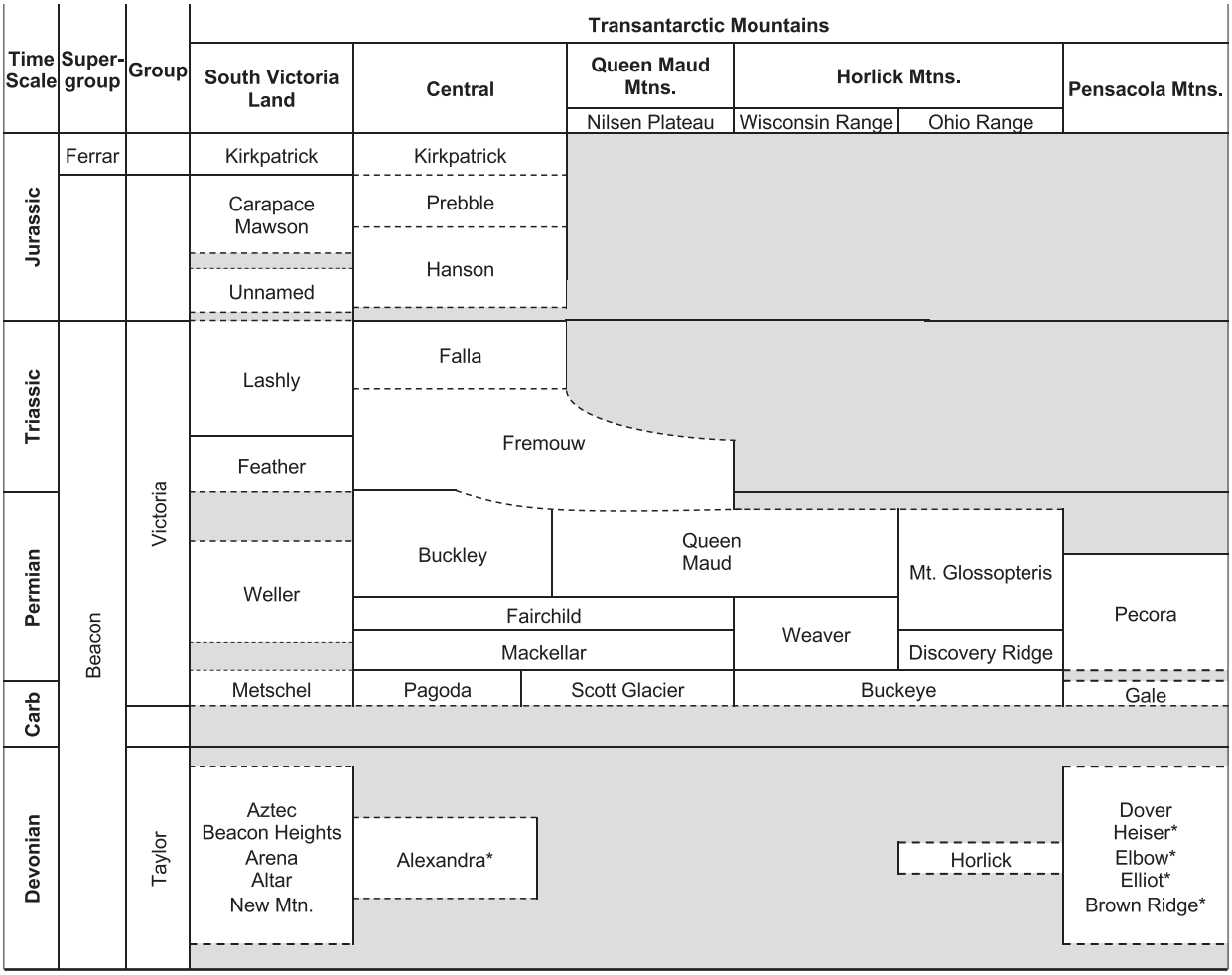

Fig. 2. Stratigraphy of the Beacon Supergroup. Compiled from Elliot (2013), Elliot et al. (2017), Collinson et al. (1994), Long (1964, 1965), and J. L. Isbell (personal communication). Carb = Carboniferous, Mtns. = Mountains, Mtn. = Mountain. Relative thicknesses approximated. *indicates uncertain age. (Modified from Sanders and Rimmer, 2020).

2.3. Geochemical analyses (C,H,N)

Geochemical analyses (C, H, N) were performed on a subset of samples (74) by ALS Global using high-temperature tube furnace combustion / TC and IR detection according to ASTM D5373 (ASTM, 2008) using a LECO TruSpec Macro. To remove any carbonates formed during intrusion, samples were treated prior to analysis with 6 N HCl following procedures described in Sanders and Rimmer (2020). All data are reported on a dry-ash free (daf) basis for HCl-treated samples, using moisture (as-received) and ash (dry) values (HCl-treated samples) previously reported in Sanders and Rimmer (2020) (Table 1).

2.4. Carbon isotopic analysis and organic carbon content

For $\delta^{13}C_{org}$ and C_{org} analysis (127 samples), approximately 2 mg of minus 230-mesh sample were placed in a silver capsule and treated with 6% sulfurous (H_2SO_3) acid to remove carbonate. The samples were dried at 80 °C and the process was repeated several times to ensure complete removal of carbonate. The capsules were analyzed at the University of Texas at Arlington Stable Isotope Laboratory using a Costech 4010 elemental analyzer coupled, via a Conflo IV Device, to a ThermoFinnigan Delta V isotope-ratio mass spectrometer; carbon isotopic values were standardized to V-PDB scale for $\delta^{13}C$ using IAEA-8573 and IAEA-8574 (glutamic acid) international standards (Table 1). The average standard deviation for $\delta^{13}C$ was 0.04‰ for the unknowns; for % C_{org} the average standard deviation was 0.02% for the unknowns.

3. Results

3.1. Petrographic analyses

Most of the samples are characterized by very high reflectances (R_r, % in oil), being either natural anisotropic cokes (e.g., some samples from the Buckely Fm. at Graphite Peak, Fig. 1), anthracites, or meta-anthracites (Fig. 3). Only four samples have reflectances below 1.5%, and two of these appear to be slightly weathered based on their fractured appearance and vitrinite discoloration (Fig. 4a); these four samples are from the Buckley Fm. from Mt. Bowers and Solitary Peak (Fig. 1). The range in R_r (%) for the Buckley Fm. is 0.53–7.58% (Table 1), with these samples showing a bimodal distribution. The range in R_r (%) for the Mt. Glossopteris Fm. is somewhat less (2.36%–3.62%), as is that for the Queen Maud Fm. (1.71%–3.35%) and the Weller Coal Measures (1.95%–2.36%) (Table 1). Mean maximum reflectances (R_{max}, % in oil) are high, ranging from 2.19% to as much as 9.73% in some of the coked Graphite Peak samples. The difference in reflectance between maxima and minima indicates a high degree of anisotropy, up to >5.5% (Table 1).

The primary constituents of these coals are vitrinite, anisotropic coke, and inertinite (especially lower reflectance semi-inertinite) (Table 1) (Fig. 4a–i). A gradual decrease in semi-inertinite and a concomitant increase in vitrinite occurs with increased rank due to the

Table 1
Geochemical and petrographic data for Antarctic samples. Ash* = ash yield (wt%, dry basis), raw samples; samples with Ash* values in bold indicate carbonaceous shales rather than true coals. All remaining geochemical data are for HCl-treated samples: Moist = moisture, wt%; Ash = ash yield, dry basis wt%; VM = volatile matter (wt%, dry, ash-free (daf) basis); C, H, and N all on a wt% daf basis; H/C and N/C based on daf values; C_{org} = organic carbon, wt%; $\delta^{13}C_{org}$, ‰. R_r, R_{max}, R_{min} = random, maximum, minimum (respectively) vitrinite reflectance (%, in oil). All petrographic data are on a vol% mineral-free basis: Vit = vitrinite, Anis = anisotropic coke, S-In = semi-inertinite, In = inertinite, PyC = pyrolytic carbon.(Note: Ash, Mois, and VM data from Sanders and Rimmer, 2020).

Sample		Name	Ash*	Moist	Ash	VM	C	H	N	H/C	N/C	C_{org}	$\delta^{13}C$	R_r	R_{max}	R_{min}	Vit	Anis	S-In	In	PyC
Buckley Formation																					
PRR-	6345	Coalsack Bluff	15.22	6.95	14.94	18.21	87.57	2.37	1.68	0.32	0.02	68.92	−23.90	3.78	4.41	3.35	53.0	0.0	43.3	2.4	1.3
PRR-	6346	Coalsack Bluff	23.39	6.30	22.76	16.42	88.48	2.31	1.69	0.31	0.02	62.32	−23.13	3.96							
PRR-	6360	Coalsack Bluff	26.09	4.48	25.73	14.95	90.20	2.30	1.49	0.30	0.01	62.76	−23.75	4.04							
PRR-	14795	Coalsack Bluff	40.99	1.61	40.25	18.44						50.64	−23.47	2.50							
PRR-	**6862**	**Mt. Achernar**	**71.74**									20.86	−23.30								
PRR-	6864	Mt. Achernar	26.57									48.44	−22.82	2.87							
PRR-	6898	Mt. Achernar	8.24	10.61	7.53	23.45	83.09	1.77	1.27	0.25	0.01	70.47	−22.83	3.30	4.35	2.57	62.3	0.0	34.0	3.3	0.4
PRR-	13731	Mt. Achernar	31.30	5.15	30.11	19.14	85.20	3.02	2.08	0.42	0.02	53.87	−23.60	2.86							
PRR-	13732	Mt. Achernar	32.93	6.45	32.21	23.50	84.05	2.14	1.97	0.30	0.02	48.19	−23.89	3.35			83.3	0.0	15.9	0.3	0.5
PRR-	13733	Mt. Achernar	16.87	10.92	15.67	15.50	95.21	0.52	1.22	0.06	0.01	59.51	−25.14	6.35	8.13	3.44	86.9	0.0	9.0	2.4	1.7
PRR-	13734	Mt. Achernar	20.25	3.65	20.24	10.84	90.79	2.88	2.00	0.38	0.02	67.35	−22.40	3.09							
PRR-	5381	Mt. Angier	7.79	7.58	6.81	21.76	85.24	2.60	2.18	0.36	0.02	71.88	−24.95	2.45			85.7	0.0	11.9	2.4	0.0
PRR-	5257	Lamping Peak	38.95									43.34	−25.49								
PRR-	**5225**	**Mt. Bowers**	**83.35**									9.67	−23.38	0.78							
PRR-	5228	Mt. Bowers	6.45	4.99	5.90	24.43	85.42	3.87	1.98	0.54	0.02	77.87	−22.31	1.43			53.1	0.0	40.6	5.9	0.4
PRR-	7075	Wahl Glacier	18.56	6.03	17.55	20.86	83.56	3.19	1.73	0.46	0.02	65.68	−24.45	2.04	2.19	1.94	69.5	0.0	26.8	3.0	0.7
PRR-	7082	Wahl Glacier	37.97									42.84	−24.80								
PRR-	6959	Mt. Picciotto	17.16	7.54	13.60	7.26	97.97	0.41	0.41	0.05	0.00	62.61	−24.93	6.93	7.75	4.36	93.7	0.0	4.8	0.8	0.7
PRR-	**6969**	**Mt. Picciotto**	**66.83**									23.76	−23.91								
PRR-	6973	Mt. Picciotto	44.28									43.64	−24.98								
PRR-	6987	Mt. Picciotto	39.82									37.89	−26.31								
PRR-	**6989**	**Mt. Picciotto**	**73.19**									16.83	−24.90								
PRR-	**7005**	**Mt. Ropar**	**55.73**									31.03	−23.84	4.91							
PRR-	7008	Mt. Ropar	10.53											4.41							
PRR-	7011	Mt. Ropar	7.97	8.71	5.85	18.57	86.57	1.76	1.38	0.24	0.01	67.21	−21.06	3.69	4.56	2.88	47.7	0.0	50.6	0.9	0.8
PRR-	**7016**	**Mt. Ropar**	**57.64**									29.51	−24.15								
PRR-	6941	Solitary Peak	10.59	14.20	9.05	41.66	73.93	2.54	1.72	0.41	0.02	57.53	−23.01	0.53			10.4	0.0	88.3	1.3	0.0
PRR-	6945	Solitary Peak	8.23	9.27	3.98	29.99	81.04	2.54	1.71	0.37	0.02	70.01	−23.89	1.08			26.8	0.0	66.5	6.5	0.2
PRR-	**14531**	**Graphite Peak**	**97.35**									2.81	−25.35								
PRR-	**14532**	**Graphite Peak**	**91.98**									3.61	−25.52								
PRR-	**14533**	**Graphite Peak**	**93.73**									4.03	−25.27								
PRR-	**14534**	**Graphite Peak**	**90.66**									5.16	−25.32								
PRR-	**14535**	**Graphite Peak**	**86.58**									8.75	−25.38								
PRR-	14536	Graphite Peak	49.07	15.38	49.26	18.36	84.99	1.21	0.54	0.17	0.01	41.36	−25.19	6.62							
PRR-	14537	Graphite Peak	32.17	1.21	31.29	4.98						64.93	−24.65	6.65	8.78	4.59					
PRR-	14538	Graphite Peak	30.12	1.23	29.84	4.58						69.76	−24.90	6.95	8.37	4.62					
PRR-	**14539**	**Graphite Peak**	**53.88**	2.67	52.52	6.75	94.56	0.28	0.39	0.04	0.00	43.82	−25.17	6.53			0.0	86.8	6.3	4.6	2.3
PRR-	14540	Graphite Peak	35.67	0.40	33.10	4.77						62.59	−24.61	5.58							
PRR-	**14541**	**Graphite Peak**	**68.94**	2.05	68.25	11.09	92.00	0.61	0.35	0.08	0.00	29.04	−24.91	6.31							
PRR-	14542	Graphite Peak	41.57	1.18	32.35	4.60						57.20	−24.54	6.27							
PRR-	**14543**	**Graphite Peak**	**60.51**									38.67	−24.87	6.42							
PRR-	14544	Graphite Peak	33.15	0.28	31.86	3.08						65.69	−24.47	7.14	9.53	5.13	0.0	86.1	7.3	5.3	1.3
PRR-	14545	Graphite Peak	24.54	0.38	23.40	2.75						80.89	−24.59	7.19	9.73	4.16	0.0	90.2	5.6	3.6	0.6
PRR-	14546	Graphite Peak	27.30	0.48	26.54	3.05						76.90	−23.98	7.54	9.45	4.78					
PRR-	**14548**	**Graphite Peak**	**80.05**	2.19	80.35	11.69	99.30	0.34	0.31	0.04	0.00	16.37	−25.33	7.58							
PRR-	**14550**	**Graphite Peak**	**83.62**									11.49	−25.69								
PRR-	**14551**	**Graphite Peak**	**73.98**	3.54	73.17	11.19	99.29	0.29	0.31	0.03	0.00	23.83	−25.07	7.04							
PRR-	**14571**	**Graphite Peak**	**68.03**	7.14	68.42	34.41	76.42	1.33	1.36	0.21	0.02	22.80	−23.47	2.62							
PRR-	14572	Graphite Peak	46.88	11.97	46.77	33.75	77.00	1.17	1.22	0.18	0.01	36.69	−22.59	1.95							
PRR-	**14573**	**Graphite Peak**	**71.44**	8.24	71.46	40.05	71.86	1.06	1.53	0.18	0.02	20.78	−22.38	2.22							

(*continued on next page*)

Table 1 (*continued*)

Sample		Name	Ash*	Moist	Ash	VM	C	H	N	H/C	N/C	C_{org}	$\delta^{13}C$	R_r	R_{max}	R_{min}	Vit	Anis	S-In	In	PyC
PRR-	**14574**	**Graphite Peak**	**67.38**	10.09	67.37	32.49	75.81	1.61	1.74	0.25	0.02	23.53	−22.65	2.08							
PRR-	**14575**	**Graphite Peak**	**92.92**									4.15	−23.69								
PRR-	**14577**	**Graphite Peak**	**87.12**	1.75	80.79	9.47	94.52	0.39	0.26	0.05	0.00	17.84	−25.22	2.79							
PRR-	**14608**	**Graphite Peak**	**75.48**	6.11	76.88	16.74	87.80	0.00	0.41	0.00	0.00	20.26	−25.28	2.80							
PRR-	**14609**	**Graphite Peak**	**84.89**									10.69	−25.96								
PRR-	**14610**	**Graphite Peak**	**83.97**									13.22	−25.45								
PRR-	**14611**	**Graphite Peak**	**93.44**									4.40	−25.67								
PRR-	**14635**	**Graphite Peak**	**69.85**	10.10	69.48	30.47	75.55	1.31	0.58	0.21	0.01	20.67	−25.66	2.60							
PRR-	**14639**	**Graphite Peak**	**83.28**									10.19	−26.54								
PRR-	**14641**	**Graphite Peak**	**55.29**	13.03	54.39	19.45	84.48	0.69	0.61	0.10	0.01	32.89	−25.87								
PRR-	14666	Graphite Peak	34.27	3.31	34.64	16.63						55.98	−25.85	1.90							
PRR-	**14667**	**Graphite Peak**	**91.81**									7.62	−25.48								
PRR-	14668	Graphite Peak	40.40	16.50	39.89	18.60	87.60	0.57	0.52	0.08	0.01	45.69	−25.48	1.84			89.0	0.0	9.6	0.0	1.4
PRR-	**14670**	**Graphite Peak**	**51.82**	13.38	52.00	21.42	79.56	0.75	0.46	0.11	0.00	36.52	−25.91	2.28			88.4	0.0	10.6	0.0	1.0
Mt. Glossopteris Formation																					
PRR-	**11393**	**Higgins Canyon**	**64.30**									31.55	−24.78								
PRR-	11539	Mt. Glossopteris	26.39	4.76	25.93	13.02	90.44	2.85	1.28	0.37	0.01	65.18	−22.83	2.69			46.2	0.0	51.3	2.0	0.5
PRR-	11541	Mt. Glossopteris	27.93	5.21	27.01	16.82	85.41	3.22	1.34	0.45	0.01	55.06	−21.98	2.50	4.27	1.88	72.3	0.0	24.0	3.5	0.2
PRR-	11693	Mt. Glossopteris	14.58	5.96	13.60	18.71	84.80	2.48	1.50	0.35	0.02	65.97	−23.26	2.56							
PRR-	11696	Mt. Glossopteris	40.07									46.72	−22.81								
PRR-	11710	Mt. Glossopteris	45.05									39.06	−23.51								
PRR-	13752	Mt. Glossopteris	11.11	5.66	10.47	19.88	83.99	3.00	1.43	0.43	0.01	72.41	−22.49	2.39							
PRR-	13753	Mt. Glossopteris	17.71	6.36	16.95	19.96	85.51	2.89	1.44	0.40	0.01	64.65	−22.81	2.40							
PRR-	13754	Mt. Glossopteris	21.54	6.55	21.25	20.58	83.08	3.16	1.63	0.45	0.02	61.68	−23.36	2.40							
PRR-	13759	Mt. Glossopteris	38.58	5.00	38.08	14.62	89.74	3.32	1.44	0.44	0.01	55.84	−23.00	2.36							
PRR-	13760	Mt. Glossopteris	24.41	5.79	17.89	17.09	86.12	2.99	1.71	0.41	0.02	51.18	−22.98	2.75			82.9	0.0	11.3	5.6	0.2
PRR-	13761	Mt. Glossopteris	19.99	5.56	19.43	16.59	85.39	2.98	1.68	0.42	0.02	64.40	−23.42	2.85							
PRR-	13763	Mt. Glossopteris	28.20	5.94	27.91	20.27	86.29	2.81	1.68	0.39	0.02	58.75	−22.74	2.81			82.9	0.0	14.9	1.7	0.5
PRR-	**13764**	**Mt. Glossopteris**	**52.08**									40.14	−22.70								
PRR-	13766	Mt. Glossopteris	30.02									49.77	−23.32								
PRR-	11435	Mt. Schopf	45.49									42.39	−23.33								
PRR-	11525	Mt. Schopf	13.28	8.13	11.59	21.40	83.39	2.38	1.38	0.34	0.01	62.06	−23.33	2.66			88.2	0.0	10.4	1.4	0.0
PRR-	13749	Mt. Schopf	32.71	7.66	31.89	20.74	83.60	2.36	1.64	0.34	0.02	50.30	−23.15	2.51							
PRR-	13750	Mt. Schopf	21.60	7.70	21.13	20.82	84.12	2.50	1.50	0.35	0.02	54.47	−22.98	3.14			89.2	0.0	8.4	2.4	0.0
PRR-	13751	Mt. Schopf	23.41	7.29	22.51	19.24	85.70	1.65	1.22	0.23	0.01	60.88	−22.28	3.62							
PRR-	13755	Mt. Schopf	13.25	5.55	13.26	14.72	86.90	3.34	1.77	0.46	0.02	70.50	−23.25	2.63			85.6	0.0	12.0	2.2	0.2
PRR-	13768	Mt. Schopf	22.79	7.29	22.40	21.73	84.15	2.06	1.43	0.29	0.01	54.02	−23.63	3.25							
Queen Maud Formation																					
PRR-	12519	Crack Bluff	25.89	4.60	24.50	17.05	85.84	2.58	1.93	0.36	0.02	58.70	−23.10	3.35			75.8	0.0	22.2	1.7	0.3
PRR-	11001	Mt. Weaver	6.65	5.83	5.13	19.58	85.67	3.23	1.95	0.45	0.02	75.20	−22.94	1.99							
PRR-	11003	Mt. Weaver	4.14	8.65	4.60	21.65	87.90	3.17	2.10	0.43	0.02	80.42	−23.24	2.11							
PRR-	11005	Mt. Weaver	20.75	4.85	20.38	17.82	86.53	2.95	1.99	0.41	0.02	68.58	−22.69	2.20							
PRR-	11012	Mt. Weaver	16.50	5.88	15.70	19.92	85.57	3.09	2.04	0.43	0.02	62.49	−23.74	1.98							
PRR-	11035	Mt. Weaver	13.59									67.76	−23.38	3.81							
PRR-	11070	Mt. Weaver	10.39	7.25	9.82	21.04	84.50	3.38	1.81	0.48	0.02	72.96	−23.71	2.03			60.3	0.0	38.0	1.4	0.3
PRR-	11072	Mt. Weaver	9.00	7.55	8.53	21.35	84.40	3.25	1.73	0.46	0.02	75.16	−22.66	1.94							
PRR-	11074	Mt. Weaver	7.69	9.29	5.02	22.62	83.10	3.29	2.03	0.47	0.02	71.10	−23.70	1.92							
PRR-	11076	Mt. Weaver	4.49	6.24	3.27	20.58	84.87	2.79	1.47	0.39	0.01	70.66	−23.16	1.79							
PRR-	11080	Mt. Weaver	8.40	6.34	6.19	20.53	83.64	2.81	1.80	0.40	0.02	75.67	−22.81	1.81							
PRR-	11105	Mt. Weaver	14.40	5.79	14.42	19.90	83.89	3.12	2.01	0.44	0.02	66.30	−22.75	1.87							
PRR-	11106	Mt. Weaver	12.51	5.92	12.37	20.16	84.56	3.19	2.05	0.45	0.02	70.24	−23.34	1.85			68.7	0.0	29.4	1.9	0.0
PRR-	11108	Mt. Weaver	5.95	6.42	5.17	21.52	82.82	3.10	1.95	0.45	0.02	74.61	−23.24	1.82							

(*continued on next page*)

Table 1 (*continued*)

Sample		Name	Ash*	Moist	Ash	VM	C	H	N	H/C	N/C	C_{org}	$\delta^{13}C$	R_r	R_{max}	R_{min}	Vit	Anis	S-In	In	PyC
PRR-	11110	Mt. Weaver	5.10	7.91	4.80	21.63	83.52	3.09	1.94	0.44	0.02	77.26	−22.44	1.78							
PRR-	11113	Mt. Weaver	9.44	7.89	5.74	21.78	83.53	3.15	2.21	0.45	0.02	81.65	−23.36	1.71							
PRR-	11114	Mt. Weaver	2.67	6.48	2.11	22.18	83.21	3.16	2.11	0.45	0.02	77.37	−23.47	1.88			86.9	0.1	11.9	0.9	0.2
PRR-	11117	Mt. Weaver	3.97	6.56	4.04	20.32	83.10	3.16	2.16	0.45	0.02	80.37	−23.43	1.81							
PRR-	11123	Mt. Weaver	12.33	5.54	11.78	19.29	85.97	3.10	2.26	0.43	0.02	69.64	−25.90	1.88							
PRR-	11126	Mt. Weaver	23.25	4.98	22.26	20.21	85.52	3.17	1.85	0.44	0.02	57.99	−23.44	1.93			59.7	0.0	38.2	1.8	0.3
PRR-	11131	Mt. Weaver	9.76	5.28	9.43	18.02	85.59	3.19	2.05	0.44	0.02	74.14	−22.32	2.09							
PRR-	11136	Mt. Weaver	17.11	5.62	16.55	19.36	83.87	2.99	1.98	0.42	0.02	64.50	−22.47	2.21							
PRR-	**11140**	**Mt. Weaver**	**81.53**									16.96	−22.94								
Weller Coal Formation																					
PRR-	13730	Allan Hills	11.13	6.10	6.05	15.33	85.45	2.94	2.02	0.41	0.02	70.24	−24.80	2.36			81.9	0.0	14.6	2.9	0.6
PRR-	**14375**	**Allan Hills**	**61.69**									34.75	−25.96								
PRR-	14377	Allan Hills	37.38									44.10	−25.66								
PRR-	14378	Allan Hills	47.14	1.37	44.73	16.24						47.06	−25.57	2.26							
PRR-	**14379**	**Allan Hills**	**52.58**	4.37	49.93	19.50						42.42	−25.19	2.02			33.6	0.0	63.4	3.0	0.0
PRR-	14381	Allan Hills	35.76	1.16	34.46	14.20						56.31	−25.28	2.01							
PRR-	**14382**	**Allan Hills**	**87.99**									7.53	−25.16								
PRR-	**14383**	**Allan Hills**	**89.60**									6.07	−24.82								
PRR-	**14384**	**Allan Hills**	**62.35**	4.28	60.95	23.39	81.86	3.53	2.09	0.51	0.02	31.48	−25.20								
PRR-	14385	Allan Hills	40.94	1.74	39.51	16.80						50.49	−25.74	2.16							
PRR-	**14386**	**Allan Hills**	**76.65**	5.37	75.33	31.49	75.43	3.89	2.36	0.62	0.03	17.61	−25.85	2.11							
PRR-	**14390**	**Allan Hills**	**87.37**									7.20	−25.24								
PRR-	**14392**	**Allan Hills**	**87.75**									6.68	−24.42								
PRR-	14393	Allan Hills	41.31	1.67	38.37	16.14						53.15	−25.16	1.95			67.0	0.0	31.0	2.0	0.0
PRR-	19051	Allan Hills	26.38	21.87	16.90	18.29						50.18	−23.13	2.28			93.3	0.0	5.7	0.9	0.1
PRR-	13703	Shapeless Mtn	27.32	10.86	22.10	14.26	87.24	2.33	0.95	0.32	0.01	50.17	−22.42	3.50	4.74	2.62	79.4	0.0	18.6	1.8	0.2
PRR-	13704	Mt. Feather	13.71	5.26	10.67	14.43	87.14	3.10	1.93	0.42	0.02	69.25	−22.68	2.37			55.3	0.0	42.8	1.2	0.7
PRR-	13700	Mt. Fleming	33.48									40.16	−23.30								
PRR-	11848	Mt. Gran	35.93									50.29	−23.79								

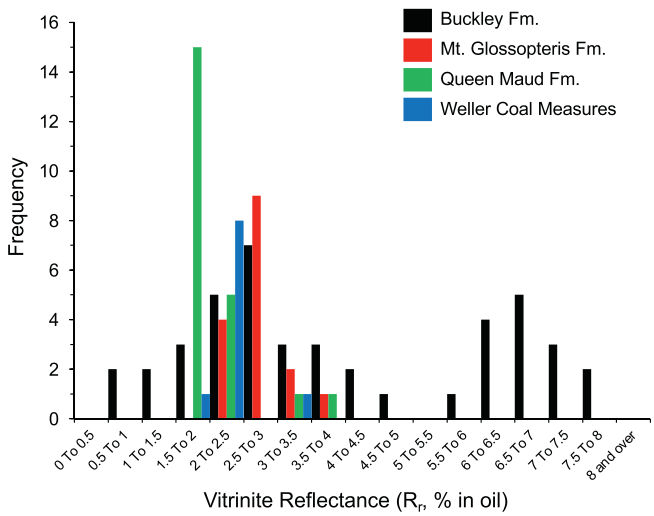

Fig. 3. Histogram showing range in mean random vitrinite reflectance (R_r, % in oil) for each formation.

increased difficulty in differentiating the two at the very highest reflectances. At this very high rank, liptinites no longer fluoresce and are usually difficult to see except in samples where their reflectance surpasses that of the vitrinite or where they occur in close association with inorganics and abundant inertinites. Well-developed anisotropic mosaic structures (coarse-grained circular and fine-grained lenticular) occur in some of the coked vitrinite (Fig. 4i). In other samples, the coke mosaic structures are less pronounced, but vitrinite anisotropy is very well developed and is readily apparent during stage rotation. Pyrolitic carbon occurs in many of the samples as a minor component (<2.5%), especially the higher rank samples, in a variety of forms including coarse grained ribbon structures, infilled vacuoles, and rims around inertinite (Fig. 4e, f).

3.2. Geochemical analyses (C,H,N)

Although many samples were classified as coals in the original field notes, upon further inspection, many are carbonaceous shales and siltstones (i.e., <50% organic matter). Organic carbon (%, C_{org}) ranges from 2.8 to 81.6% (Table 1, Fig. 5). Most cluster between 50% and 80%, but many samples, especially those from the Buckley Fm., are <40%, with the Buckley samples showing a bimodal distribution. As ash yield (%, dry) is quite variable (2–80%), C, H, and N results were converted to a dry, ash-free (daf) basis. Note that data calculated to a dry, mineral-matter-free (dmmf) basis would incorporate error as the Parr formula used to calculate to this basis (mineral matter = 1.08Ash% - 0.55S%) makes assumptions about mineral content that are not valid for these samples as they contain little to no pyrite and S is present as gypsum (Sanders and Rimmer, 2020). Rank-sensitive parameters show the wide range in organic maturity of these samples, with C (%, daf)) contents between 71.9 and 99.3%. The data show a strong negative correlation ($r = -0.902$, significant at the 1% level) with previously reported volatile matter data (VM, % daf, HCl-treated samples, as reported in Sanders and Rimmer, 2020) (Fig. 6a). Hydrogen values (%, daf) decrease from ~2.4 to 0%, N (%, daf) ranges from 2.36 to 0.26%, and a strong correlation exists between the two variables ($r = 0.873$, significant at the 1% level) (Fig. 6b). The Buckely Fm. samples exhibit the widest range of values. These results confirm the very high rank of the samples indicated by the vitrinite reflectance data, particularly for several Buckley Fm. samples primarily from Graphite Peak that plot close to the origin (Fig. 6b).

3.3. Isotopic analyses

The overall range in $\delta^{13}C_{org}$ for the Antarctic samples is −26.5‰ to −21.1‰ (5.4‰ range) and shows a bimodal distribution (Table 1) (Fig. 7). The ranges for the coal-bearing formations are −26.5‰ to −21.1‰ for the Buckley Fm.; −24.8‰ to −22.0‰ for the Mt. Glossopteris Fm.; −25.9‰ to −22.3‰ for the Queen Maud Fm.; and − 26.0‰ to −23.1‰ for the Weller Coal Measures. The two populations of values are centered around 1) –23.5 to −23‰ that includes samples from all four formations, and 2) –25.5 to −25‰ that mostly includes samples from the Buckley Fm. and the Weller Coal Measures. The widest range in $\delta^{13}C_{org}$ is observed in the Buckley Fm., which is characterized also by the widest range in vitrinite reflectance (Fig. 8). Many of the samples with the more depleted values were collected from the Buckley Fm. at Graphite Peak. Focusing in on the relationships between $\delta^{13}C_{org}$ and other variables for the Buckley Fm., a significant relationship exists between total inertinite content (inertinite plus semi-inertinite) and $\delta^{13}C_{org}$ ($r = 0.678$, significant at the 1% level), with higher total inertinite contents associated with more enriched values (Fig. 9a). Furthermore, a significant relationship occurs between $\delta^{13}C_{org}$ and the H/C atomic ratio ($r = 0.589$, significant at the 1% level) (Fig. 9b). Although the relationship between H/C atomic ratio and the amount of pyrolytic carbon is significant ($r = -0.705$, significant at the 1% level) (Fig. 9c), indicating increased pyrolytic carbon with increased rank, the relationship between pyrolytic carbon and $\delta^{13}C_{org}$ is less clear ($r = -0.424$, not significant at the 5% level) (Fig. 9d). Despite the significant correlations in these relationships, considerable scatter in the data occurs, suggesting multiple controls.

4. Discussion

4.1. Petrographic and geochemical observations

Two important petrographic observations are made for the Antarctic coals: one dealing with composition, the other with rank. Like many Permian-age southern hemisphere coals (e.g., Snyman and Botha, 1993; Taylor et al., 1998; Cairncross, 2001) these samples are relatively high in inertinite content, particularly semi-inertinite, which averages ~26% and reaches up to 88%. Much of the semi-inertinite is what is referred to as reactive semi-fusinite, typical of South African Permian coals (Falcon, 1986), material that has slightly higher reflectance than the accompanying vitrinite. While other possible origins have been suggested for the inertinite macerals funginite and macrinite (e.g., bacterial and fungal activity) (Hower et al., 2009, 2011, 2013), a wildfire origin is most likely for semifusinite, fusinite, and inertodetrinite (Guo and Bustin, 1998; Scott and Glasspool, 2007; Hudspith et al., 2012; Moroeng et al., 2018). The high inertinite content of Antarctic and other Late Permian coals (Diessel, 2010) is consistent with high atmospheric O_2 levels, possibly as high as 24% (Berner, 2006), that likely contributed to extensive fire activity during this time (Berner and Canfield, 1989).

In addition to the inertinite macerals, significant amounts of vitrinite (av. ~63%) and anisotropic coke (av. ~8%), and small amounts of pyrolytic carbon are also present. A few occurrences of coked bitumen are also observed (Sanders and Rimmer, 2020). Whereas no liptinite was counted, trace amounts of highly altered meta-liptinite were observed (Sanders and Rimmer, 2020). It is likely that these coals originally contained some liptinite, as has been observed in other lower rank Antarctic coals (e.g., Bauer et al., 1997; Holdgate et al., 2005) and other coals in South Africa (e.g., Falcon and Snyman, 1986; Kruszewska, 2003; Wagner et al., 2019). In the case of sub-bituminous to high volatile bituminous Permian coals from East Antarctica, liptinite content can be as high as 20–30% (Holdgate et al., 2005). The significance of the varied petrographic composition of these coals with respect to carbon isotopic data is discussed below.

Petrographic analysis indicates that the majority of the coals were altered extensively by heat associated with burial maturation and, in

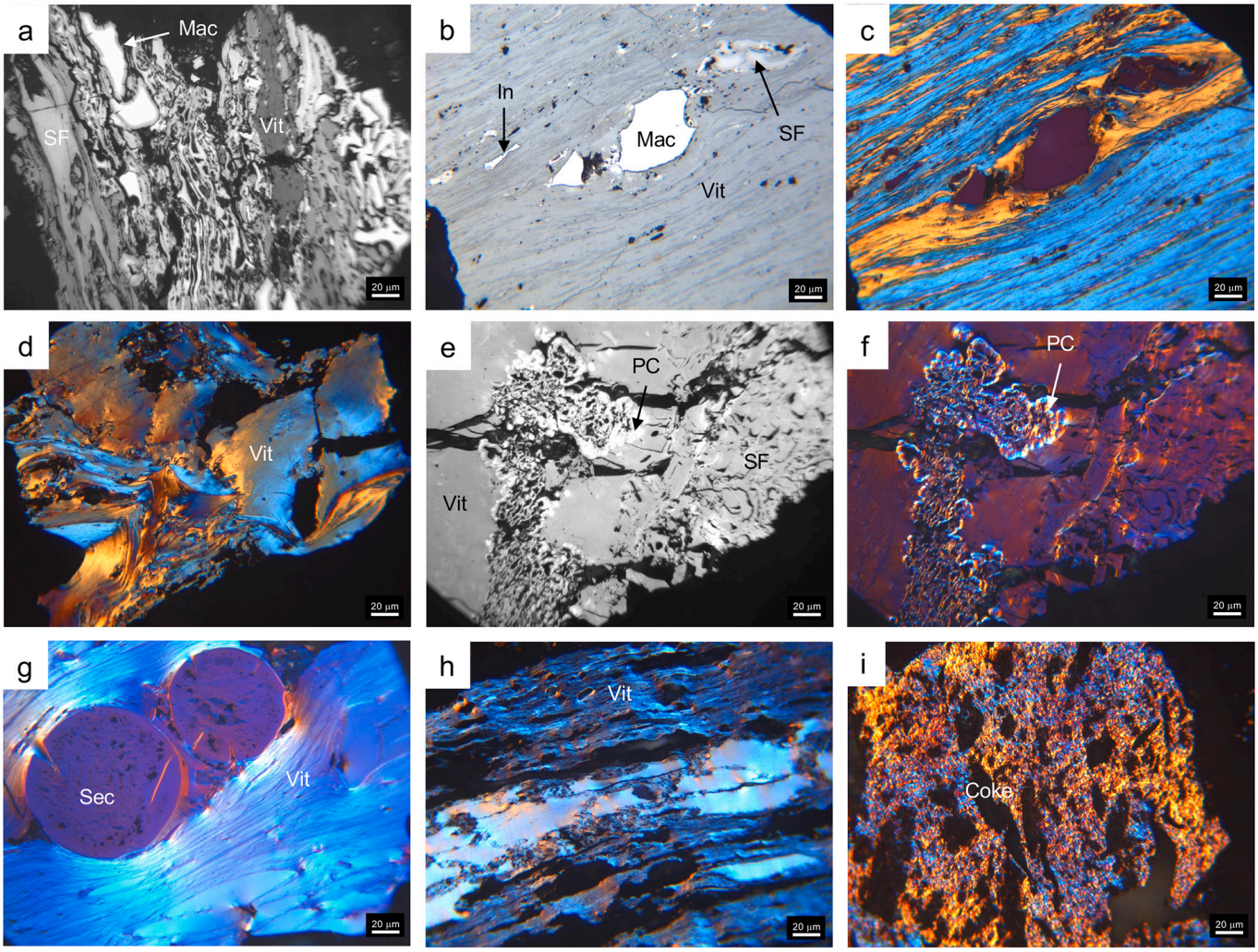

Fig. 4. Petrographic features observed in Antarctic coals. All photomicrographs taken in reflected white-light. Images c, d, f, g, h, and i taken using crossed polarizers and an antiflex objective. a) PRR-6941, Buckley Fm., Solitary Peak, (R_r = 0.53%), vitrinite (Vit), semifusinite (SF), and macrinite (Mac), note the presence of some oxidized, fractured rims on some inertinites; b) PRR-11525, Mt. Glossopteris Fm., Mt. Schopf (R_r = 2.66%), macrinite (Mac), inertodetrinite (In), semifusinite (SF), and altered vitrinite (Vit); c) same field of view (approx.) as (b); d) PRR-11525, Mt. Glossopteris Fm., Mt. Schopf (R_r = 2.66%), altered vitrinite (Vit); e) PRR-7011, Buckley Fm., Mt. Ropar (R_r = 3.69%), altered vitrinite (Vit), semifusinite (SF), and pyrolytic carbon (PC); f) same field of view as (e); g) PRR-13703, Weller Coal Fm., Shapeless Mtn. (R_r = 3.50%), altered vitrinite (Vit) and secretinite (Sec); g) PRR-13733, Buckley Fm., Mt. Arachner (R_r = 6.35%), altered vitrinite (Vit); i) PRR-14546, Buckley Fm., Graphite Peak (R_r = 7.54%), anisotropic coke (Coke) with abundant devolatilization vacuoles.

many cases, contact metamorphism. Of the samples measured, vitrinite reflectance analysis demonstrates 25% are low volatile bituminous, ~37% are semi-anthracite, 13% are anthracite, and 20% are meta-anthracite or anisotropic coke. The anisotropic cokes are vesiculated and show primarily coarse-grained circular and fine-grained lenticular mosaic textures, formed by the rapid heating of coal that was medium volatile bituminous in rank at the time of intrusion (maximum vitrinite reflectance ~1.2%) (Sanders and Rimmer, 2020). Initial rank increase was due to normal burial maturation, to depths of 4–5.5 km (Sanders and Rimmer, 2020) under estimated geothermal gradients of between 25 and 34 °C for the TAM (Fitzgerald, 1992, 1994; Lisker and Läufer, 2013). Emplacement of Jurassic-age sills and dikes led to coke formation in those coals in close proximity to the intrusions (R_r up to 7%); for non-coked coals, further rank increase to current levels (~2.5% R_r) was due to continued burial maturation (Sanders and Rimmer, 2020). The pyrolytic carbon represents gases that were devolatilized during the rapid heating associated with contact metamorphism, cracked, and redeposited upon cooling (Taylor et al., 1998; Kwiecińska and Patersen, 2004; Kwiecińska and Pusz, 2016). Its presence suggests exposure to extremely high temperatures, as high as 500 °C (Goodarzi et al., 1993) or 600 °C (Chandra and Taylor, 1982). The presence of vacuoles in the coke further suggests rapid devolatilization.

Contact-metamorphosed coals show significant chemical changes including a decrease in VM, increase in C, and decrease in H and N (e.g., Stewart et al., 2005; Gröcke et al., 2009; Rimmer et al., 2009; Presswood et al., 2016) along with an increase in aromaticity and decrease in aliphatic content (Fredericks et al., 1985; Presswood et al., 2016), and can reach vitrinite reflectances >5% (Rimmer et al., 2009; Sanders and Rimmer, 2020). Geochemical results for the Antarctic samples confirm the high rank of the samples and offer evidence for devolatilization. Considerable loss of VM in the coals occurred with increased rank (Fig. 6a) and along with this, loss of H and N (Fig. 6b). Despite the considerable decrease in VM, it is well known that the R_r–VM trend for intruded coals does not follow that of coals matured by normal burial maturation (e.g., Pearson and Murchison, 1999; Murchison, 2004, 2006), with VM contents consistently higher than normal at R_r levels >2% (Rimmer et al., 2009), and this trend is seen in the Antarctic coals where the intruded samples have VM contents that are several percent higher than normal (see Fig. 10 in Sanders and Rimmer, 2020). Similarly, the relationship between VM and C differs from that seen in non-

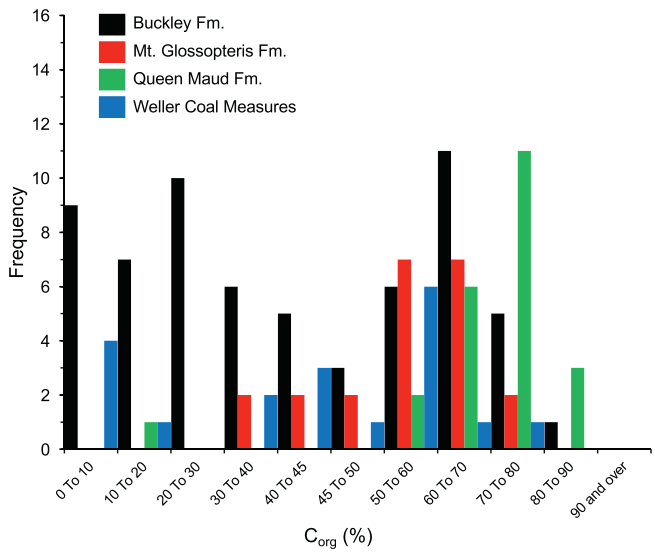

Fig. 5. Histogram showing range in C_{org} (%) for samples from each formation.

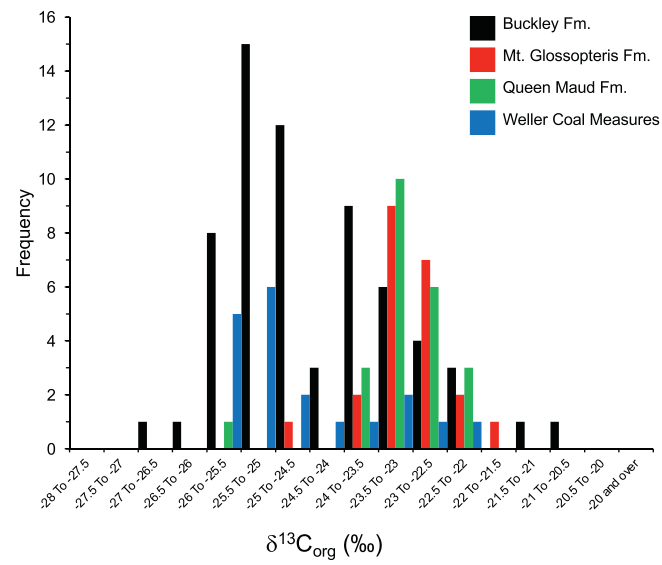

Fig. 7. Histogram showing range in $\delta^{13}C_{org}$ (‰) for each formation.

intruded coals. For example, several Buckley Fm. coals have VM contents of ~12% (daf) at a C content of ~91% (daf) (the boundary between semi-anthracite and anthracite coal) (Table 1), whereas coals that have undergone normal burial maturation would have VM contents of ~8% at this C content (based on data in Taylor et al., 1998). It is possible that released VM in the intruded coals was trapped, either due to the rapid heating rate (Crelling and Dutcher, 1968) or in the extensive pore structure within the contact aureole (Gurba and Weber, 2001; Saghafi et al., 2008).

4.2. Possible influences on $\delta^{13}C_{org}$ of Antarctic coals

The original $\delta^{13}C_{org}$ value of terrestrial OM is determined by several factors such as the type and age of the plants when they were buried, the plant organ from which the material is derived, climatic conditions during the growth of the plant, latitude, altitude, and amount of relative humidity (Arens et al., 2000, and references therein; Gröcke, 2002; Dawson et al., 2002; Diefendorf et al., 2010; Kohn, 2010; Schubert and Jahren, 2012). Arens et al. (2000) concluded that 90% of the variability in $\delta^{13}C_{org}$ values of C3 plant tissue is due to the $\delta^{13}C$ value of the atmosphere and is not due to environmental factors or differences in the plant life. However, OM preserved in shales and coals may have gone through many compositional changes from the time of accumulation to

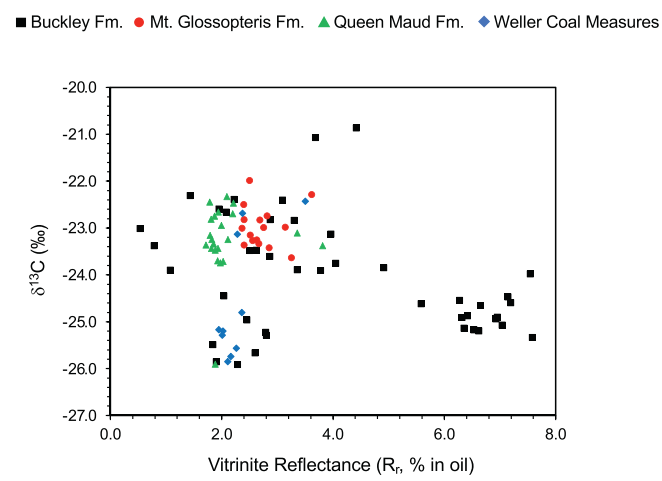

Fig. 8. Relationship between $\delta^{13}C_{org}$ and mean random vitrinite reflectance (R_r, % in oil) for each formation,

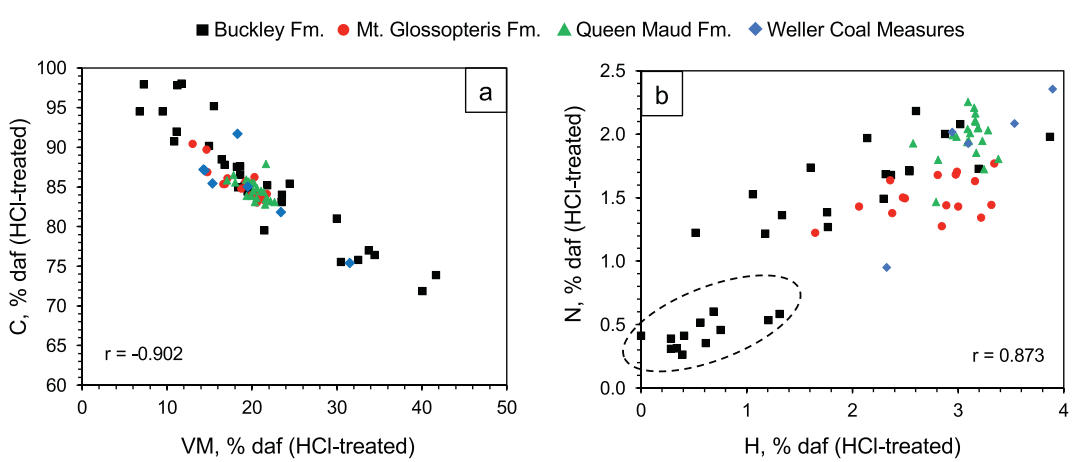

Fig. 6. Relationship between a) VM and C; b) N and H. All data are on a dry, ash-free (daf) basis (HCl-treated samples). Very low H and N samples in dashed area in Fig. 6b include samples from Graphite Peak and one sample from Mt. Picciotto.

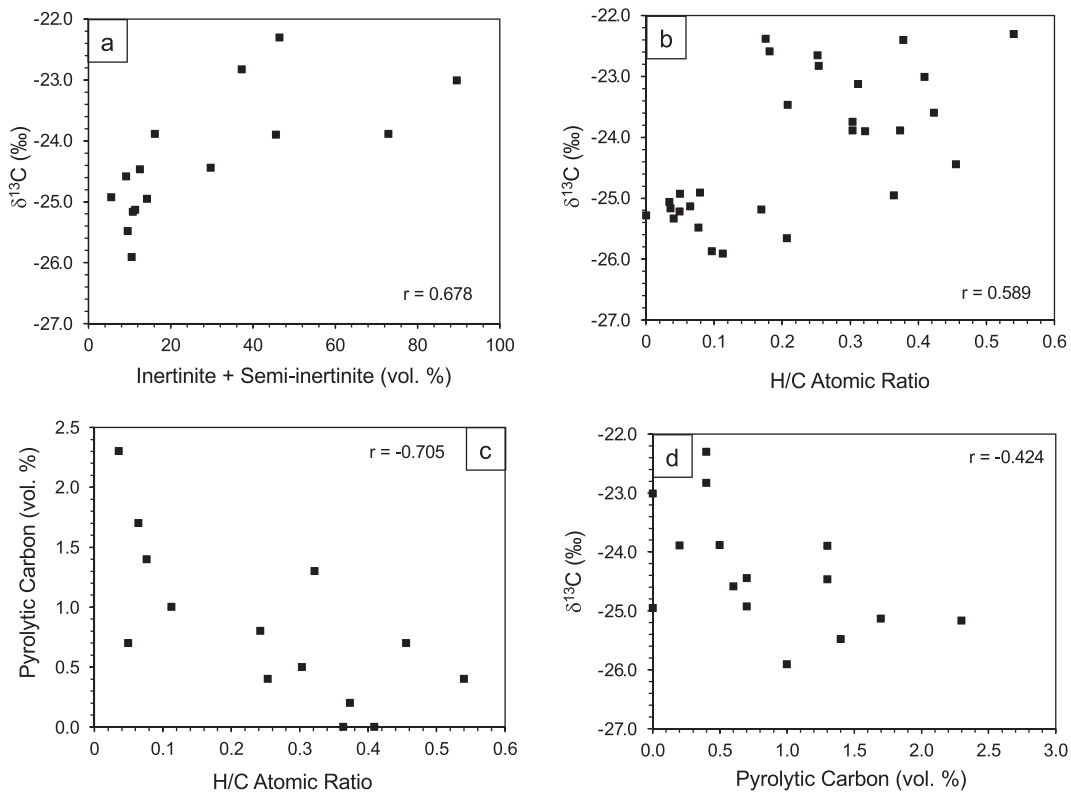

Fig. 9. Selected relationships between variables for Antarctic samples. a) $\delta^{13}C_{org}$ and inertinite + semi-inertinite (vol%), Buckley Fm.; b) $\delta^{13}C_{org}$ and H/C atomic ratio (daf basis), Buckley Fm.; c) H/C atomic ratio (daf basis) and pyrolytic carbon content (vol%), Buckley Fm.; d) $\delta^{13}C_{org}$ and pyrolytic carbon content (vol%) (all samples).

the present including early alteration within the peat swamp or sediments, possible release of biogenic CH_4, coal maturation through anthracite rank and beyond, including possible generation and migration of bitumen/oil and late-stage biogenic CH_4 generation, intrusion, and weathering. Carbon isotopic composition can be altered by surface exposure and oxidation of OM (Petsch et al., 2003) and more lipid-rich components are more susceptible to weathering than more refractory macerals (Slater, 2009). However, weathering due to surface exposure after the uplift of the TAM does not seem to have affected the Antarctic coals to any great extent, perhaps because the coals were of such high rank prior to being exposed at the surface and because of the very cold climate (Schopf and Long, 1966). Previous work has shown that coals collected from the outcrop surface do not differ greatly geochemically from those taken 12 ft below the surface (Schopf and Long, 1966). Assuming weathering was not a factor for the Antarctic coals, other processes should be considered that may have affected the OM over time. Possible factors include variations in original types of components (ultimately, macerals), diagenetic and metamorphic changes, and size of the carbon reservoir. Despite the degree of scatter in the Antarctic $\delta^{13}C_{org}$ data when plotted against parameters such as rank, petrographic composition, and carbon content, significant correlation coefficients exist between these variables, suggesting that such factors variably and collectively control the bulk isotopic composition.

4.2.1. Maceral composition

The typical range in carbon isotopic composition of coal is between −22‰ to −27‰, and within a coal, different macerals have different isotopic compositions with more enriched values observed for vitrinites and inertinites compared to the more depleted values observed for liptinitic macerals (Whiticar, 1996). Generally, liptinites are derived from materials that have isotopic compositions that are ~2‰ more depleted than those that formed from woody tissues (i.e., vitrinite). Furthermore, inertinites like fusinite that are derived primarily from fire-affected sources (i.e., fossil charcoal) are at least ~0.5‰ enriched relative to vitrinite. Using density-gradient separation of a single Pennsylvanian-age coal, Rimmer et al. (2006) demonstrated that individual macerals show at least a 2.9‰ difference in $\delta^{13}C_{org}$ values (Fig. 10a). As the separates were not entirely pure in the lowest density fractions, this difference is potentially slightly larger, >3‰. A clear relationship exists between $\delta^{13}C_{org}$ and C/H atomic ratio (Fig. 10b), with the changes in C/H reflecting the decrease in aliphatic and increase in aromatic components of the different macerals across the density gradient (Rimmer et al., 2006). For Miocene lignites, Bechtel et al. (2002, 2008) reported a negative relationship between liptinite content and $\delta^{13}C_{org}$ (Fig. 10c). These authors estimated that a 40% contribution from liptinite (as one would see in a cannel coal, e.g., alginite, sporinite) could produce a ~2‰ decrease in $\delta^{13}C_{org}$. In a study of four Chinese sections across the Permian–Triassic boundary, Wu et al. (2021) provided data for hand-picked cuticles (cutinite), wood (vitrinite), and charred wood (inertinite), and showed that $\delta^{13}C_{org}$ values for cutinite are typically 1–2‰ more depleted than those of the vitrinite. Conversely, Dal Corso et al. (2011) reported a wide distribution of $\delta^{13}C_{org}$ values (2–5‰) for Late Triassic amber (resinite), and an enrichment of ~2.5‰ compared to associated wood. Thus, the type of liptinite is important in addition to the amount present. Inertinite content may also influence $\delta^{13}C_{org}$. In combustion experiments, Jones and Chaloner (1991) reported an enrichment of 0.5–0.8‰ due to charcoalification of woody tissues, and as much as ~1.5‰ at high temperatures. In a study of intruded high-volatile bituminous Gondwanan coals of the Karoo Basin, Gröcke et al. (2009) found that maceral composition, specifically inertinite content, rather than rank increase influenced $\delta^{13}C_{org}$. The influence of inertinite macerals on $\delta^{13}C_{org}$ in coals from the Karoo Basin was further demonstrated by Moroeng et al. (2018), showing more enriched values in coals with higher inertinite contents (Fig. 10d).

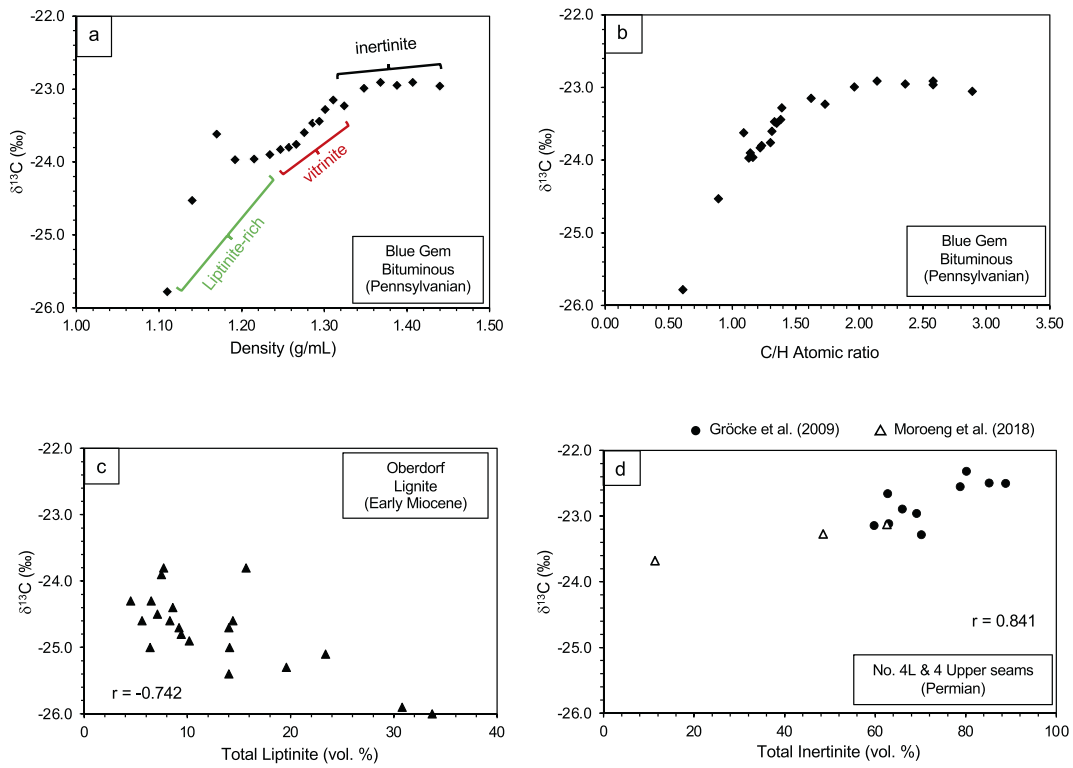

Fig. 10. Influence of maceral composition on $\delta^{13}C_{org}$. a) $\delta^{13}C_{org}$ values for different density fractions, with dominant macerals indicated (Blue Gem coal, Pennsylvanian, Appalachian Basin, USA) (data from Rimmer et al., 2006); b) $\delta^{13}C_{org}$ versus C/H atomic ratio for density fractions of the Blue Gem coal (data from Rimmer et al., 2006); c) relationship between total liptinite content (vol%) and $\delta^{13}C_{org}$ for the Early Miocene Oberdorf lignite (Styrian Basin, Austria) (data from Bechtel et al., 2002); d) relationship between total inertinite content (vol%) and $\delta^{13}C_{org}$ for Permian No. 4 L and No. 4 Upper Seam (Karoo Basin, South Africa) (data from Gröcke et al., 2009, and Moroeng et al., 2018).

For the Antarctic coals, little to no liptinite is recorded due to the high rank of the coals, with the exception of a few lower rank samples. The fact that any liptinite was altered should be considered when attempting to tie $\delta^{13}C_{org}$ for coalified materials back to original atmospheric conditions. It is one line of evidence that the maceral composition, and thus the isotopic composition, changed following peat accumulation and organic maturation. Variations in the amount of total inertinite versus vitrinite may also be a factor in carbon isotopic composition, although the difference between these two macerals is rather small. It is also possible that secondary macerals (those that form after peat accumulation) such as pyrolytic carbon may also be a factor. In the Antarctic coals, more pyrolytic carbon is observed in higher rank coals and cokes, as demonstrated by the inverse relationship seen with H/C (Fig. 9c). In a study of Raton Basin coals, Cooper et al. (2007) reported abundant pyrolytic carbon adjacent to sill contacts; this material would have accumulated from ^{12}C-rich volatile matter released from the coals at the time of sill intrusion and may be responsible for the more depleted $\delta^{13}C_{org}$ values observed at sill contacts in their study. Other studies of Raton Basin coals also showed $\delta^{13}C_{org}$ of samples close to a sill are more depleted than expected (Meyers and Simoneit, 1999), a signature attributed to the immobilization of pyrolysis products and accumulation of secondary carbon forms. Similarly, intruded coals from the Piceance Basin included pyrolytic carbon close to the sill contacts and some also showed more depleted $\delta^{13}C_{org}$ values (Rimmer, unpublished data).

These studies point to the importance of determining the petrographic composition of samples that are analyzed for $\delta^{13}C_{org}$, and for petrographic composition to be considered when evaluating changes in $\delta^{13}C_{org}$ in the rock record, especially when minor excursions (on the order of 1–2‰) are concerned. This problem is not limited to terrestrial environments, and could be even more pronounced in marine sections where both marine and terrestrial components, each with different $\delta^{13}C_{org}$ values, contribute to the bulk $\delta^{13}C_{org}$ signature. For example, based on palynological analysis, variability in the relative amounts of marine versus terrestrial components and in the different types of terrestrial plant groups can explain both negative and positive bulk $\delta^{13}C_{org}$ values across the Triassic–Jurassic boundary rather than a global carbon isotope event (van de Schootbrugge et al., 2008). An examination of many published isotope curves for CIEs such as the Permian–-Triassic boundary show considerable scatter in bulk $\delta^{13}C_{org}$ signatures, and the variability introduced by different plant components (which are maceral precursors) contributes to the noise in the $\delta^{13}C_{org}$ signal; data from Wu et al. (2021) are shown as an example (Fig. 11). Whereas there is obviously a change in $\delta^{13}C_{org}$ values at the boundary, the size of the change is debatable due to the scatter in the data. Such variability leads us to concur with Robinson and Hesselbo (2004) who suggested that chemostratigraphic studies should be limited to a single specific plant organ (such as wood, charcoal, cuticles, etc.) (e.g., Bacon et al., 2011) or, in the case of coal, a specific lithotype (e.g., Van de Wetering et al., 2019); clearly, organic petrology can provide important insights (e.g., Storm et al., 2022).

4.2.2. *Organic maturation and size of the carbon reservoir*

With an increase in coal rank, only small changes in $\delta^{13}C_{org}$ are observed at relatively low levels of maturation. For example, Whiticar (1996) reported that between 0.6% and 1.3% R_r, liptinites and vitrinites became enriched by 1‰, but no change was observed in inertinites; similarly, Mastalerz and Schimmelmann (2002) reported an enrichment of 1‰ for coals between 0.5 and 1.7% R_r, and Boudou et al. (1984) reported an enrichment of 2‰ with an increase in rank (0.5 to 2.0% R_r). The absence of a large shift in $\delta^{13}C_{org}$ over the lignite–anthracite rank range is thought to be due to to the very large carbon reservoir

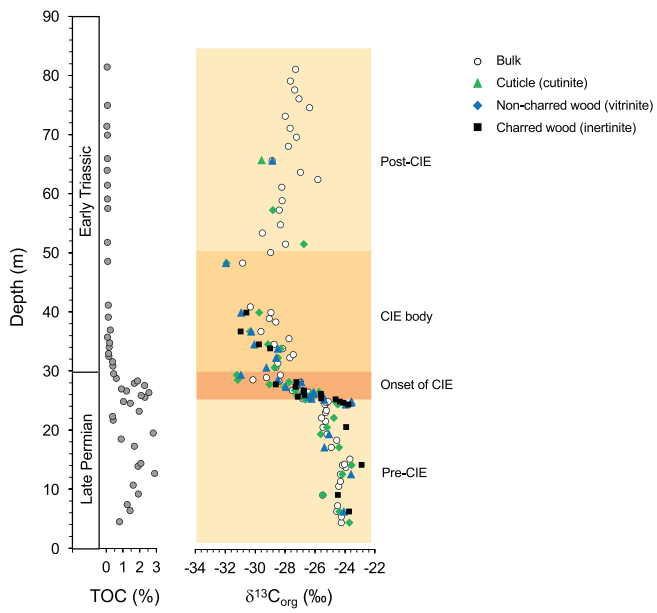

Fig. 11. $\delta^{13}C_{org}$ values for bulk organic matter, cuticle (~cutinite), uncharred wood (~vitrinite), and charred wood (~inertinite) across the CIE associated with the Permian–Triassic boundary for the Chinahe section, eastern Yunnan, SW China (data from Wu et al., 2021). Note the high degree of variability in $\delta^{13}C_{org}$ values for the different plant constituents, especially at the onset of the CIE.

represented by coal and the fact that relatively little carbon is lost as CH_4 over this rank range (Sackett, 1978; Whiticar, 1996).

At very high levels of maturation, however, significant changes in $\delta^{13}C_{org}$ may be observed. In meta-anthracites, $\delta^{13}C_{org}$ values for coal become more enriched (McKirdy and Powell, 1974; Hoefs and Frey, 1976; Whiticar, 1996) due to the liberation of CH_4, which is depleted (25‰ more negative than coal) as the CH_4 incorporates more ^{12}C than ^{13}C (Hoefs and Frey, 1976; Sackett, 1978). For example, Hoefs and Frey (1976) reported $\delta^{13}C_{org}$ values of −10 to −15‰ for metamorphosed OM, compared to −24 to −28‰ for unmetamorphosed material. It is reasoned that, because ^{12}C—^{12}C bonds would be easier to break than ^{13}C—^{12}C, any CH_4 released would have a $\delta^{13}C_{org}$ composition that is more depleted, and the organic residue would become enriched in the heavier isotope (Hoefs and Frey, 1976; Conkright and Sackett, 1992; Schimmelmann et al., 2009). Between VM contents of 40–20%, approximately equal volumes of CO_2 and CH_4 are released but beyond that, into anthracite levels, only CH_4 is released in substantial quantities (Jüntgen and Karweil, 1966). Thus, at temperatures <100–150 °C, little change in coal $\delta^{13}C_{org}$ would be expected, but at temperatures ≥200 °C, coal $\delta^{13}C_{org}$ should enrich due to the release of depleted CH_4 (Hoefs and Frey, 1976). Thus, enriched $\delta^{13}C_{org}$ values should be seen in the residual coal when temperatures exceeded 200 °C (or $R_r \geq 2.2\%$). When heated to 400 °C, bituminous coals with an average $\delta^{13}C_{org}$ of ~ −23‰ showed little change in $\delta^{13}C_{org}$ values in a semi-closed system, but significant enrichment in ^{13}C of the coal residue in an open system (as much as an 8.4–9.8‰ difference) due to the loss of ^{13}C-depleted gases (including light *n*-alkanes and CH_4) (Ciesielczuk et al., 2021). Thus, the degree of openness of the geological system is also critical.

Antarctic coals are thought to have been exposed to temperatures ~140–150 °C prior to emplacement of the Ferrar dikes, sills, and lava flows, resulting in coal that was high to medium volatile bituminous at the time of intrusion, possibly followed by further heating to ~200–210 °C post intrusion (Sanders and Rimmer, 2020). Coals close to the intrusions would have been impacted by rapid heating to much higher temperatures, perhaps as high as 500–600 °C assuming an intrusion temperature of 1200 °C (Bauer et al., 1997), but at least 450–500 °C based on the production of mesophase and anisotropic mosaic structures (Taylor, 1961; Brooks and Taylor, 1968; Crelling, 2008). Thus, small changes on the order of 1–2‰ from the original values could be expected in Antarctic samples not directly impacted by contact metamorphism, but much greater changes may be expected in coals that were in close contact with the intrusions. However, several previous studies (e.g., Cooper et al., 2007; Gröcke et al., 2009; Schimmelmann et al., 2009; Yoksoulian, 2010; Yoksoulian et al., 2016; Rahman et al., 2017) demonstrated that trends in $\delta^{13}C_{org}$ in coals intruded by dikes are somewhat ambiguous (Fig. 12a), often showing a sinusoidal pattern. These examples include Pennsylvanian high-volatile bituminous coals (Schimmelmann et al., 2009; Yoksoulian, 2010; Yoksoulian et al., 2016; Rahman et al., 2017), high-volatile bituminous, inertinite-rich Permian coals (Gröcke et al., 2009), and high- to medium-volatile bituminous Cretaceous coals (Cooper et al., 2007; Yoksoulian, 2010). The only significant difference seen between these isotope transects is that the Permian-age coals have $\delta^{13}C_{org}$ values that are ~2‰ more enriched than the others, which may in part reflect their high inertinite content (~60–85%), and are consistent with $\delta^{13}C_{org}$ values reported for Late Permian coals from South Africa (e.g., Faure et al., 1995; Moroeng et al., 2018).

Reasons for the less-than-expected changes in $\delta^{13}C_{org}$ in intruded coals may be complex. This could be related, in part, to the large size of the carbon reservoir (Whiticar, 1996). Studies that have shown a significant change in $\delta^{13}C_{org}$ for intruded rocks are based on samples that have very low initial carbon contents. For example, Hoefs and Frey (1976) described a 14‰ isotopic change in metamorphosed samples that contain <3% C_{org}, with the majority containing <1%; thus, the effects of ^{12}C loss were more pronounced on the residue. The range in C_{org} for the Antarctic coals and carbonaceous shales is considerable (~3–82%) (Fig. 5), with many of the Buckley Fm. samples <40%, but none are as low as 1–2%. Except for a few outliers, there is a significant relationship between $\delta^{13}C_{org}$ and C_{org} (Fig. 13a), suggesting that the size of the carbon reservoir may be important. Late Permian age samples from Graphite Peak analyzed previously (Krull and Retallack, 2000) showed extremely depleted $\delta^{13}C_{org}$ values but only in low C_{org} samples (<0.1% C_{org}); the majority of samples with C_{org} contents >1% are within the expected range −22 to −26‰ (Fig. 13b). Thus, in low carbon samples, the possibility of both rank effects and maceral variability potentially come into play. For the depleted values reported for the Buckley Fm., Krull and Retallack (2000) cited an H/C of 0.46 and C_{daf} of 67% (according to Coates et al., 1990), and thus appropriately discounted rank affects that occur at temperatures >350 °C that could alter carbon isotopic composition. However, Coates et al. (1990) only reported analyses for a single sample from this location and the calculation of the values reported in Krull and Retallack (2000) was unclear. Our results for the Buckley Fm. at Graphite Peak (15 samples) show an average H/C ratio of 0.11 and an average C_{daf} of 85% (with several values >90%), values that are consistent with our petrographic observations and R_r data. Our petrographic observations also suggest at least some samples have been exposed to temperatures as high as 500–600 °C. At these temperatures, some fractionation would be expected, and this would be most apparent in low C_{org} samples. However, such fractionation should result in enriched $\delta^{13}C_{org}$ OM, not depleted as seen here; therefore, additional factors need to be considered.

At such high temperatues pyrolytic carbon can form from volatiles released from rapidly heated organics. As mentioned above, it has been suggested that pyrolytic carbon can result in highly depleted $\delta^{13}C_{org}$ values (Meyers and Simoneit, 1999; Cooper et al., 2007) (Fig. 12b). If the $\delta^{13}C_{org}$ values of pyrolytic carbon reflect formation from volatiles such as coal-bed thermogenic CH_4 (−40‰), a small amount of pyrolytic carbon, particularly in low-carbon sedimentary rocks, could have a large effect on bulk $\delta^{13}C$ values. Differences have been noted in coals impacted by sills versus dikes: the duration of heat alteration by a sill may be greater than that caused by a dike, and a larger volume of coal would likely be impacted by the sill (Cooper et al., 2007). As such,

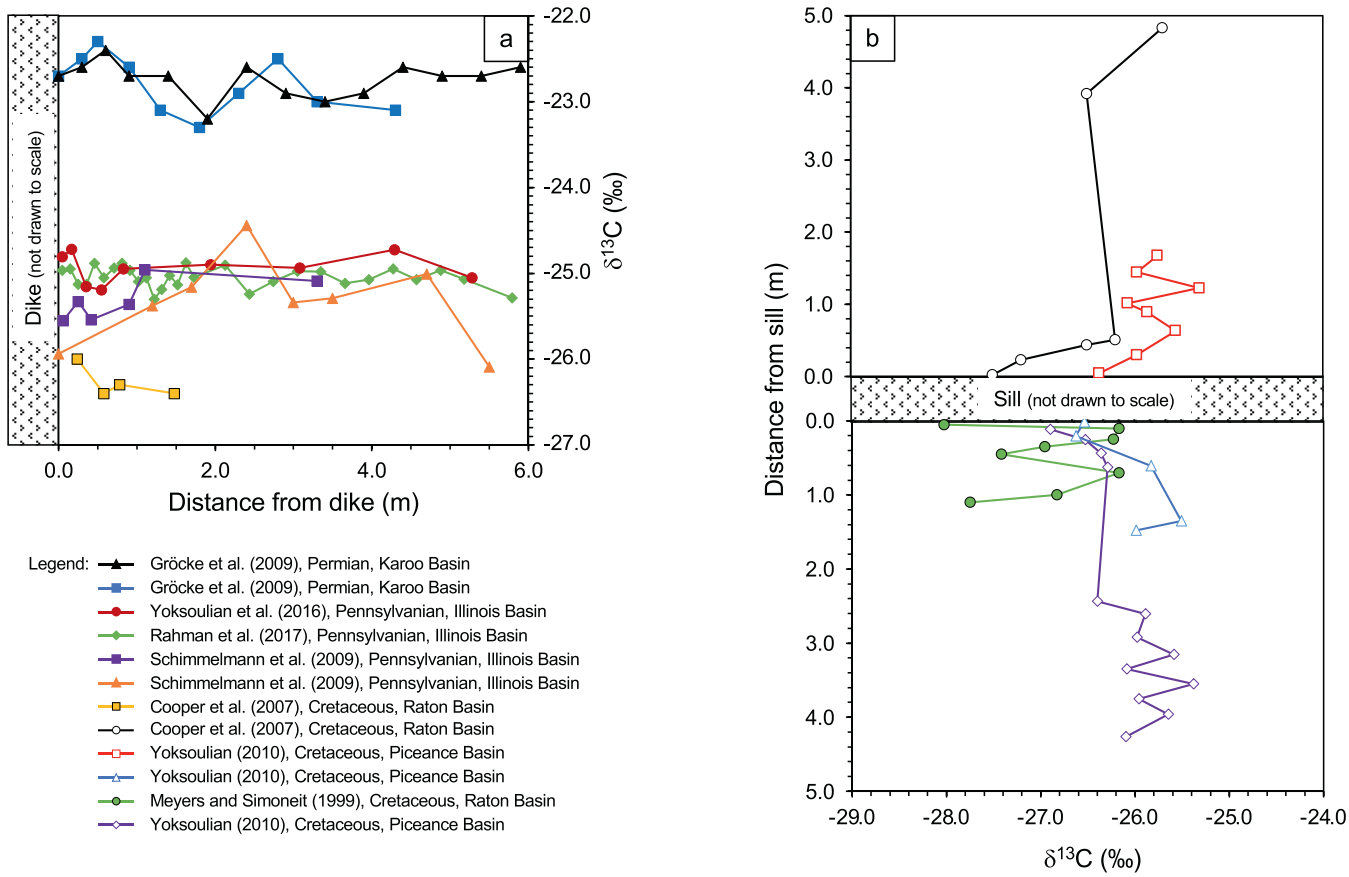

Fig. 12. $\delta^{13}C_{org}$ changes in coals adjacent to intrusions as reported in previous studies. a) carbon isotopic variations in coals intruded by dikes; b) carbon isotopic variations in coals intruded by sills.

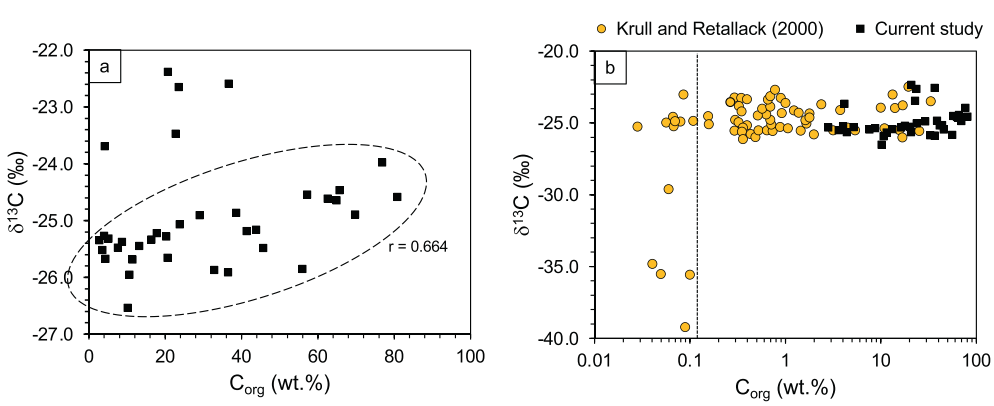

Fig. 13. a) $\delta^{13}C_{org}$ versus C_{org} for Permian Buckley Fm. samples from Graphite Peak. Note that, except for the 4 more enriched samples around −23‰ that are generally lower in reflectance (R_r ~ 2%), the remaining samples (in dashed area) show a significant correlation (at the 1% level) between the two variables; b) Comparison of $\delta^{13}C_{org}$ and C_{org} of the Permian Buckley Fm. samples at Graphite Peak with previously reported data for other Permian samples from that locale (data extracted from Fig. 3A in Krull and Retallack, 2000).

pyrolytic carbon may be more prevalent adjacent to sills and contribute to depleted $\delta^{13}C$ values (Fig. 12b).

Several studies of isotopic composition of Antarctic sections at the Permian–Triassic boundary have attempted to minimize the effects of high levels of maturation on $\delta^{13}C_{org}$ by sampling well away from known intrusions, using the 1–2× width rule (Dow, 1977; Bostick and Pawlewicz, 1984; Horner and Krissek, 1991) where the contact aureole is thought to be 1–2 times the width of the intrusion. For example, in the Allan Hills area, Retallack and Krull (1999) sampled no closer than 200 m from an 8-m thick dike, and at Graphite Peak, samples were collected in areas deemed to be "most free of intrusions". However, although care was taken to sample the least thermally altered sections of OM, petrographic analysis showed that these samples experienced extensive thermal alteration either by contact metamorphism (in the case of the coked samples) or more regional heating (in the case of the anthracites and meta-anthracites). The size of the contact aureole can be influenced by several factors beyond the width of the intrusion, including the rank of the OM at the time of intrusion (e.g., Murchison, 2006; Gröcke et al., 2009), thermal conductivity (Barker et al., 1998; Cooper et al., 2007), duration of heating (Barker et al., 1998; Cooper et al., 2007), degree of sediment compaction (Raymond and Murchison, 1988), level of water saturation (Raymond and Murchison, 1988; Gröcke et al., 2009), differing lithologies (Quaderer et al., 2016; Goodarzi et al., 2018), and whether the primary mode of heat transfer is via convection or conduction (Raymond and Murchison, 1988; Barker et al., 1998). As a result, contact aureoles may be between 0 and 7 times the width of the

intrusion (Jones and Creaney, 1977; Perregaard and Scheiner, 1979; Bostick and Pawlewicz, 1984; Saxby and Stephenson, 1987; Raymond and Murchison, 1988; Goodarzi et al., 2019). In one area of the TAM (Mt. Schopf, Ohio Range), Sanders and Rimmer (2020) noted that, based on data from Schapiro and Gray (1966), vitrinite reflectance did not attain background levels for much greater distances than 1–2 times intrusion width, an important observation as the thickness of the overlying sill was estimated to be ~177 m. In reality, it might be nearly impossible to obtain samples of coals that have not been influenced by significant burial maturation and even intrusion in many locations along the Transantarctic Mountains (Sanders and Rimmer, 2020).

Thus, controls on $\delta^{13}C_{org}$ of intruded Antarctic coals and carbonaceous shales, beyond original atmospheric composition and normal changes associated with peat accumulation and diagenesis, appear to be fairly complex and include: maceral composition, rank at the time of intrusion, extent of overall rank changes including contact metamorphism, release of volatiles and deposition of pyrolytic carbon, and size of the carbon reservoir. Despite considerable scatter, several significant correlations exist between $\delta^{13}C_{org}$ and other variables including % C_{org}, maceral composition, vitrinite reflectance, and H/C, suggesting that multiple factors influence isotopic composition, thereby elevating the importance of organic petrography in such studies. The lack of significant changes in $\delta^{13}C_{org}$ in the residual OM approaching intrusions noted in previous studies (e.g., Gröcke et al., 2009; Schimmelmann et al., 2009; Yoksoulian et al., 2016; Rahman et al., 2017) also raises a question: Is this simply due to the large size of the carbon reservoir or is the rate of alteration so rapid and at such high temperatures compared to normal burial maturation that limited fractionation of the carbon occurs as gases are evolved? Many other differences between maturation trends for normal burial and contact metamorphism have been reported (van Krevelen and Schuyer, 1957; Pearson and Murchison, 1999; Murchison, 2004, 2006; Rimmer et al., 2009; Rahman and Rimmer, 2014; Presswood et al., 2016; Rahman et al., 2017; Li et al., 2018). An additional question would be, how open was the system at the time of contact heating? It was suggested that the release of volatiles is so rapid that some cannot escape and remain in the coal (Crelling and Dutcher, 1968; Gurba and Weber, 2001; Saghafi et al., 2008).

The highly depleted $\delta^{13}C_{org}$ values reported by Retallack and coworkers for Permian samples collected close to or at the Permian–-Triassic boundary (e.g., Retallack and Krull, 1999; Retallack and Jahren, 2008) are notable in that they are limited to very low C_{org} samples (<0.1%) (Fig. 13). The samples from the current study fall within the normal background range for the area reported by Retallack and Jahren (2008) for samples with >1% C_{org} (Fig. 13). Triassic Fremouw Formation samples reported by Krull and Retallack (2000) have a wide range of $\delta^{13}C$ values, from ~ −22‰ to < −43‰; most of the very depleted samples are also very low carbon (< 0.1%). While the results presented here cannot directly explain the very large (−22.2‰) excursion found in previous studies of the Antarctic Permian–Triassic boundary (Retallack and Jahren, 2008), it is clear that the $\delta^{13}C$ excursion is evident worldwide although much smaller (e.g., Magaritz et al., 1988; Baud et al., 1989; Morante, 1996; Wignall et al., 1998; Twitchett et al., 2001; de Wit et al., 2002; Grasby and Beauchamp, 2008; Scholze et al., 2017; Bagherpour et al., 2020; Saitoh and Isozaki, 2021). However, it is possible that, due to igneous intrusion of carbonaceous shales and coals, released VM was trapped within the rocks and re-deposited as pyrolytic carbon; in very low carbon rocks this could have a measurable effect on the bulk isotopic composition. Perhaps additional work on such samples (in terms of organic petrography and rank determination) would help elucidate these highly depleted $\delta^{13}C_{org}$ values.

It is clear that $\delta^{13}C_{org}$ values of coals and other organic-bearing rocks should be interpreted carefully, as the signature reflects not only the processes that may have influenced carbon fractionation during a plant's life, such as the carbon isotopic composition of the atmosphere and ecological factors (such as water availability, altitude, temperature, etc.) (Gröcke, 1998; Arens et al., 2000), the components preserved (i.e., woody tissue, cuticles, pollen, etc.) (Gröcke, 1998), but also those processes associated with early diagenesis (Dal Corso et al., 2011) and organic maturation.

For the Antarctic samples, the accumulation and maturation history is complex (Fig. 14), with potential changes in $\delta^{13}C_{org}$ arising during 4 stages: 1) Late Permian –peat stage: atmospheric and ecological factors, preservation of different types of plants and plant organs (proto-macerals), wildfires (producing inertinite), degradation within the swamp; 2) Triassic – Early Jurassic – burial maturation: compositional changes associated with maturation through medium volatile rank (T ~ 140–150 °C), including biogenic methanogenesis, hydrocarbon generation and migration; 3) Early–Middle Jurassic – contact metamorphism: for coals in close proximity to dikes and sills, T ~ 500–600 °C, coking, extensive loss of volatiles, possible formation of pyrolytic carbon and other maceral changes, possible hydrothermal alteration; and 4) Middle Jurassic – present day: continued burial maturation, T ~ 200–210 °C, uplift, erosion, weathering. Such a complex history may result in changes to the initial $\delta^{13}C_{org}$ that may obscure trends in paleoatmospheric $\delta^{13}C$ signatures, and even produce spurious negative or positive shifts that could be misinterpreted. The magnitude of CIEs and possible sources of isotopically light carbon introduced into the atmosphere (whether from increased methanogenesis, volcanic CO_2 emissions, methane clathrate, igneous intrusion into carbonaceous reock, or other sources) are all important factors in accurate modelling of paleoatmospheric composition associated with extinction events. Inclusion of organic petrography in carbon-isotopic studies can provide important insights to changes in $\delta^{13}C_{org}$ in the rock record.

5. Conclusions

1. The majority of Late Permian Antarctic samples collected from the TAM are characterized by high levels of maturation, being low-volatile bituminous to meta-anthracite in rank. Several samples from the Buckley Fm. at Graphite Peak show signs of rapid heating due to emplacement of Jurassic-age sills and dikes, with anisotropic cokes showing coarse-grained circular and fine-grained lenticular mosaic textures that formed by intrusion of what was medium volatile bituminous coal (consistent with temperatures of ~140–150 °C and a burial depth of 4–5.5 km at the time of intrusion). The mosaic textures and the presence of pyrolytic carbon suggest temperatures at intrusion contacts were at least 450 °C and may have approached 500–600 °C. Background reflectance values at Graphite Peak (i.e., those away from intrusions) are typically ≥2%, suggesting exposure to temperatures around 200–210 °C.
2. Geochemical analyses (VM, C, H, N, and H/C) support the petrographic assessment of high rank for these samples. Values of C_{org} range between ~72% and 99%, generally consistent with the high rank suggested by the reflectance data. Values of H and N decrease with increasing C content. Values of H/C decrease from over 0.4 down to <0.1.
3. Like other Gondwanan coals, many samples are high in total inertinite content, especially reactive semi-inertinite. Liptinites are rarely observed (due to the high rank of the samples) and several samples contain pyrolytic carbon.
4. Values of $\delta^{13}C_{org}$ vary between −26.5 and −21.1‰ (5.4‰ difference) and are consistent with previously reported values for Antarctic coals. Significant correlations are observed between $\delta^{13}C_{org}$ and variables including C_{org} content, maturation parameters, and total inertinite content, although plots do show considerable scatter.
5. Due to the variability in $\delta^{13}C_{org}$ of the Antarctic sample, and the possible influence of the level of organic maturity, maceral composition, and carbon reservoir size on $\delta^{13}C_{org}$, caution should be exercised when $\delta^{13}C_{org}$ is used to interpret paleo-environmental atmospheric $\delta^{13}C$ values and extinction events.
6. This study points to the importance of incorporating organic petrography in studies of carbon isotope excursions. In particular,

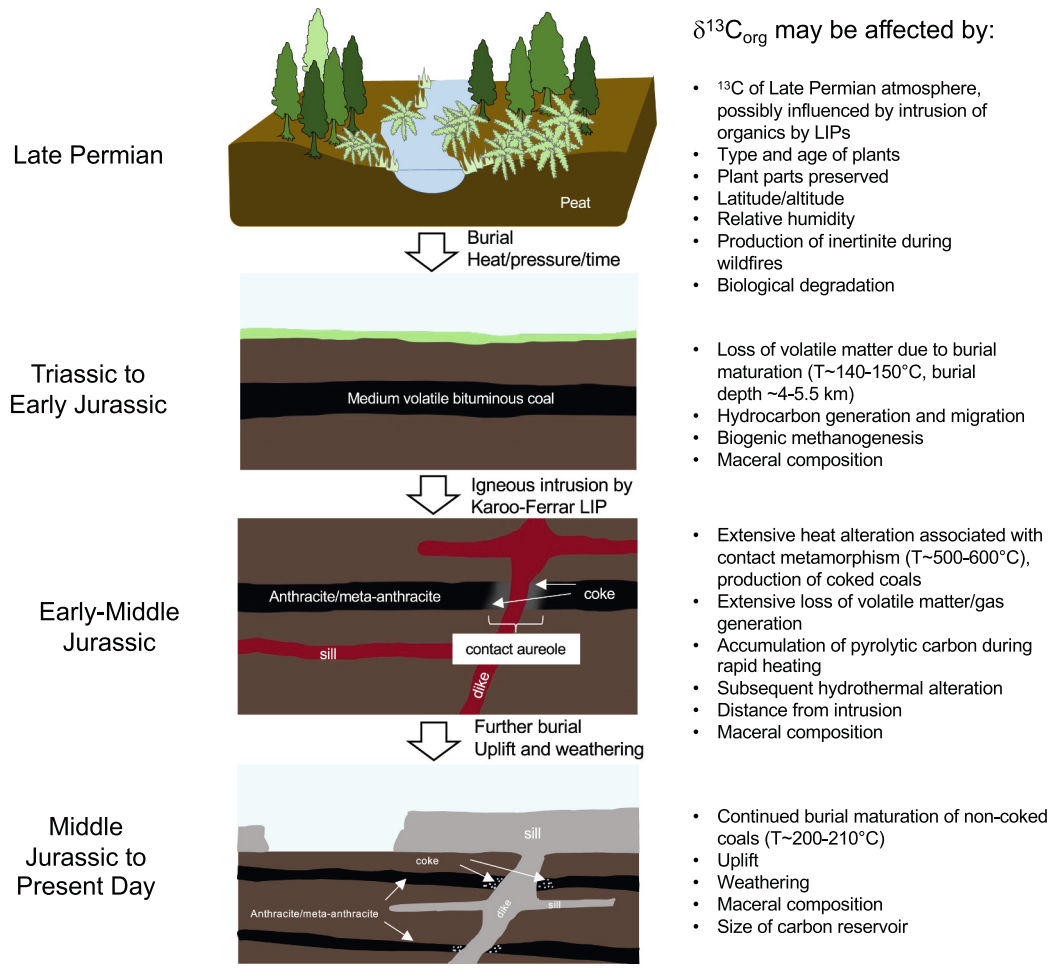

Fig. 14. Schematic diagram showing processes that could have influenced $\delta^{13}C_{org}$ in the Antarctic coal and shale samples.

rank, maceral composition, and C_{org} should be assessed as this can influence the magnitude of potential excursions. The example described herein (Antarctica) possibly represents an extreme case due to the extensive thermal alteration of the coals, but even at locales that do not show contact metamorphism, variations in OM type, amounts present, and rank are factors to be considered, especially when small CIEs are present.

Author statement

All authors contributed to the development of this project, data collection, and the writing of the manuscript.

Declaration of Competing Interest

The authors declare no conflicts of interest.

Data availability

Data will be made available on request.

Acknowledgments

This research used samples and data provided by the Polar Rock Repository (PRR), which is sponsored by the U.S. National Science Foundation Office of Polar Programs. We are also indebted to Gregory Retallack (University of Oregon) for providing coal samples from Graphite Peak and Allan Hills (samples subsequently incorporated into the PRR collection). This research was funded by NSF grants ANT–0636771 and ANT–1039365 (to SMR), the Antoinette Lierman Medlin Scholarship (Geological Society of America) (to MMS), and the Spackman Student Research Award (The Society for Organic Petrology) (to MMS). We acknowledge the Norwegian Polar Institute's Quantarctica package (base map for Fig. 1). Finally, we thank Stephen Hesselbo and an anonymous reviewer for their very helpful comments that improved the manuscript.

References

Algeo, T.J., Ellwood, B., Nguyen, T.K.T., Rowe, H., Maynard, J.B., 2007. The Permian–Triassic boundary at Nhi Tao, Vietnam: evidence for recurrent influx of sulfidic watermasses to a shallow-marine carbonate platform. Palaeogeogr. Palaeoclimatol. Palaeoecol. 252, 304–327.

Algeo, T.J., Henderson, C.M., Ellwood, B., Rowe, H., Elswick, E., Bates, S., Lyons, T., Hower, J.C., Smith, C., Maynard, B., Hays, L.E., Summons, R.E., Fulton, J., Freeman, K.H., 2012. Evidence for a diachronous Late Permian marine crisis from the Canadian Arctic region. GSA Bull. 124, 1424–1448.

Arens, N.C., Jahren, A.H., Amundson, R., 2000. Can C3 plants faithfully record the carbon isotopic composition of atmospheric carbon dioxide? Paleobiol. 26, 137–164.

ASTM, 2008. Standard D5373-08. Standard test Methods for Instrumental Determination of Carbon, Hydrogen, and Nitrogen in Laboratory Samples of Coal. ASTM International, West Conshohocken, PA. https://doi.org/10.1520/D5373–08. www.astm.org.

ASTM, 2011. Standard D2798-11a. Standard test Method for Microscopical Determination of the Vitrinite Reflectance of Coal. ASTM International, West Conshohocken, PA. https://doi.org/10.1520/D2798–11A. www.astm.org.

ASTM, 2013. Standard D2799–13.Standard Test Method for Microscopical Determination of the Maceral Composition of Coal. ASTM International, West Conshohocken, PA. https://doi.org/10.1520/D2799–13. www.astm.org.

Bacon, K.L., Belcher, C.M., Hesselbo, S.P., McElwain, J.C., 2011. The Triassic–Jurassic boundary carbon-isotope excursions expressed in taxonomicallly identified leaf cuticles. Palaios 26, 461–469.

Bagherpour, B., Bucher, H., Vennemann, T., Schneebeli-Hermann, E., Yuan, D.-x., Leu, M., Zhang, C., Shen, S.Z., 2020. Are Late Permian carbon isotope excursions of local or of global significance? GSA Bull. 132, 521–544.

Barker, C.E., Bone, Y., Lewan, M., 1998. Fluid inclusion and vitrinite-reflectance geothermometry compared to heat-flow models of maximum paleotemperature next to dikes, western onshore Gippsland Basin, Australia. Int. J. Coal Geol. 37, 73–111.

Barret, P.J., 1969. Stratigraphy and Petrology of the Mainly Fluviatile Permian and Triassic Beacon Rocks, Beardmore Glacier Area, Antarctica. Inst. of Polar Studies, Rept. 34. The Ohio State University, Columbus, OH, p. 132.

Barrett, P.J., Elliot, D.H., Lindsay, J.F., 1986. The Beacon Supergroup (Devonian-Triassic) and Ferrar Group (Jurassic) in the Beardmore Glacier area, Antarctica. In: Turner, M.D., Splettstoesser, J.F. (Eds.), Geology of the Central Transantarctic Mountains, Antarctic Research Series 36. Am. Geophys. Union, Washington, DC, pp. 339–428.

Baud, A., Magaritz, M., Holser, W.T., 1989. Permian–Triassic of the Tethys: carbon isotope studies. Geol. Rundsch. 78, 649–677.

Bauer, W., Hagemann, H.W., Poscher, G., Sachsenhofer, R.F., Spaeth, G., 1997. Permian coals from Western Dronning Maud Land - Composition, environment, and the influence of Jurassic magmatism on their maturity. In: Ricci, C.A. (Ed.), The Antarctic Region: Geological Evolution and Processes. Terra Antarctica, Siena, Italy, pp. 945–951.

Bechtel, A., Sachsenhofer, R.F., Gratzer, R., Lücke, A., Püttmann, W., 2002. Parameters determining the carbon isotopic composition of coal and fossil wood in the early Miocene Oberdorf lignite seam (Styrian Basin, Austria). Org. Geochem. 33, 1001–1024.

Bechtel, A., Gratzer, R., Sachsenhofer, R.F., Gusterhuber, J., Lücke, A., Püttmann, W., 2008. Biomarker and carbon isotope variation in coal and fossil wood of Central Europe through the Cenozoic. Palaeogeogr. Palaeoclimatol. Palaeoecol. 262, 166–175.

Berner, R.A., 2002. Examination of hypotheses for the Permo-Triassic boundary extinction by carbon cycle modeling. Proc. Natl. Acad. Sci. USA 99, 4172–4177.

Berner, R.A., 2006. GEOCARBSULF: a combined model for Phanerozoic atmospheric O_2 and CO_2. Geochim. Cosmochim. Acta 70, 5653–5664.

Berner, R.A., Canfield, D.E., 1989. A new model of atmospheric oxygen over Phanerozoic time. Am. J. Sci. 289, 172–177.

Bostick, N.H., Pawlewicz, M.J., 1984. Paleotemperatures based on vitrinite reflectance of shales and limestones in igneous dike aureoles in the Upper Cretaceous Pierre Shale, Walsenburg, Colorado. In: Woodward, J.G., Meissner, F.F., Clayton, J.L. (Eds.), Hydrocarbon Source Rocks of the Greater Rocky Mountain Region. Rocky Mtn. Assoc. Geol, pp. 387–392.

Boudou, J.-P., Pelet, R., Letolle, R., 1984. A model of the diagenetic evolution of coal sedimentary organic matter. Geochim. Cosmochim. Acta 48, 1357–1392.

Brand, U., Blamey, N., Garbelli, C., Griesshaber, E., Posenato, R., Angiolini, L., Azmy, K., Farabegoli, E., Came, R., 2016. Methane Hydrate: killer cause of Earth's greatest mass extinction. Palaeoworld 25, 496–507.

Broger, S.D., 2011. Antarctica – before and after Gondwana. Gondwana Res. 19, 335–371.

Brooks, J.D., Taylor, G.H., 1968. The formation of some graphitizing carbon. In: Walker, P.L. (Ed.), Chemistry and Physics of Carbon, 4. Marcel Dekker, NY, pp. 243–286.

Burgess, S.D., Bowring, S.A., 2015. High-precision geochronology confirms voluminous magmatism before, during, and after Earth's most severe extinction. Sci. Adv. 1, e1500470.

Cairncross, B., 2001. An overview of the Permian (Karoo) coal deposits of southern Africa. J. Afr. Earth Sci. 33, 529–562.

Campbell, I.H., Czamanske, G.K., Fedorenko, V.A., Hill, R.I., Stepanov, V., 1992. Synchronism of the Siberian traps and the Permian-Triassic boundary. Science 258, 1760–1763.

Cao, C.Q., Wang, W., Jin, Y.G., 2002. Carbon isotope excursions across the Permian-Triassic boundary in the Meishan section, Zhejiang province, China. Chin. Sci. Bull. 47, 1125–1129.

Chandra, D., Taylor, G.H., 1982. Thermally altered coals. In: Stach, E., Mackowsky, M. Th., Teichmüller, M., Taylor, G.H., Chandra, D., Teichmüller, R. (Eds.), Coal Petrology. Gebrüder Borntrager, Berlin, pp. 206–218.

Ciesielczuk, J., Górka, M., Fabia'nska, M.J., Misz-Kennan, M., Jura, D., 2021. The influence of heating on the carbon isotope composition, organic geochemistry, and petrology of coal from the Upper Silesian Coal Basin (Poland): An experimental and field study. Int. J. Coal Geol. 241, 103749.

Coates, D.A., Stricker, G.D., Landis, E.R., 1990. Coal geology, coal quality, and coal resources in Permian rocks of the Beacon Supergroup, Transantarctic Mountains, Antarctica. In: Splettstoesser, J.F., Dreschhoff, G.A.M. (Eds.), Mineral Resources Potential of Antarctica. Antarctic Res. Ser. 51, pp. 133–162.

Collinson, J.W., Isbell, J.L., Elliot, D.H., Miller, M.F., Miller, J.M.G., 1994. Permian-Triassic Transantarctic Basin. In: Veevers, J.J., Powell, C. McA (Eds.), Permian-Triassic Pangean Basins and Foldbelts along the Panthalassan Margin of Gondwanaland. GSA Mem, 184, pp. 173–222.

Collinson, J.W., Hammer, W.R., Askin, R.A., Elliot, D.H., 2006. Permian-Triassic boundary in the central Transantarctic Mountains, Antarctica. GSA Bull. 118, 747–763.

Conkright, M.E., Sackett, W.M., 1992. Stable carbon isotope changes during the maturation of organic matter. In: Whelan, J.K., Farrington, J.W. (Eds.), Organic Matter: Productivity, Accumulation, and Preservation in Recent and Ancient Sediments. Columbia University Press, New York, pp. 403–414.

Cooper, J.R., Crelling, J.C., Rimmer, S.M., Whittington, A.G., 2007. Coal metamorphism by igneous intrusion in the Raton Basin, CO and NM: implications for generation of volatiles. Int. J. Coal Geol. 71, 15–27.

Crelling, J.C., 2008. Chapter 7 - Coal Carbonization. In: Suaréz-Ruiz, I., Crelling, J.C. (Eds.), Applied Coal Petrology. Elsevier, Burlington, pp. 173–192.

Crelling, J.C., Dutcher, R.R., 1968. A petrologic study of a thermally altered coal from the Purgatoire River Valley of Colorado. GSA Bull. 79, 1375–1386.

Cridland, A.A., 1963. A Glossopteris flora from the Ohio Range, Antarctica. Am. J. Bot. 50, 186–195.

Czamanske, G.K., Gurevitch, A.B., Fedorenko, V., Simonov, O., 1998. Demise of the Siberian Plume: paleogeographic and paleotectonic reconstruction from the Prevolcanic and volcanic record, North-central Siberia. Int. Geol. Rev. 40, 95–115.

Dal Corso, J., Preto, N., Kustatscher, E., Mietto, P., Roghi, G., Jenkyns, H.C., 2011. Carbon-isotope variability of Triassic amber, as compared with wood and leaves (Southern Alps, Italy). Palaeogeogr. Palaeoclimatol. Palaeoecol. 302, 187–193.

Dawson, T.E., Mambelli, S., Plamboeck, A.H., Templer, P.H., Tu, K.P., 2002. Stable isotopes in plant ecology. Annu. Rev. Ecol. Syst. 33, 507–559.

de Wit, M.J., Ghosh, J.G., de Villiers, S., Rakotosolofo, N., Alexander, J., Tripathi, A., Looy, C., 2002. Multiple organic carbon isotope reversals across the Permo-Triassic boundary of terrestrial Gondwanan sequences: clues to extinction patterns and delayed ecosystem recovery. J. Geol. 110, 227–240.

Dickens, G.R., O'Neil, J.R., Rea, D.K., Owen, R.M., 1995. Dissociation of oceanic methane hydrate as a cause of the carbon isotope excursion at the end of the Paleocene. Paleoceanog. Paleoclimatol. 10, 965–971.

Diefendorf, A.F., Mueller, K.E., Wing, S.L., Koch, P.L., Freeman, K.H., 2010. Global patterns in leaf ^{13}C discrimination and implications for studies of past and future climate. Proc. Natl. Acad. Sci. 107 (13), 5738–5743.

Diessel, C.F.K., 2010. The stratigraphic distribution of inertinite. Int. J. Coal Geol. 81, 251–268.

Dow, W.G., 1977. Kerogen studies and geological interpretations. J. Geochem. Explor. 7, 79–99.

Elliot, D.H., 2013. The geological and tectonic evolution of the Transantarctic Mountains: A review. In: Hambrey, M.J., Barker, P.F., Barrett, P.J., Bowman, V., Davies, B., Smellie, J.L., Tranter, M. (Eds.), Antarctic Palaeoenvironments and Earth-Surface Processes, Geol. Soc. London Spec. Publ, vol. 381, pp. 7–35.

Elliot, D.H., Fleming, T.H., Kyle, P.R., Foland, K.A., 1999. Long-distance transport of magmas in the Jurassic Ferrar Large Igneous Province, Antarctica. Earth Planet. Sci. Lett. 167, 89–104.

Elliot, D.H., Fanning, C.M., Isbell, J.L., Hulett, S.R.W., 2017. The Permo-Triassic Gondwana sequence, central Transantarctic Mountains, Antarctica: zircon geochronology, provenance, and basin evolution. Geosphere 13, 155–178.

Erwin, D.H., 1993. The Great Paleozoic Crisis: Life and Death in the Permian. Columbia Univ. Press, 327 pp.

Erwin, D.H., 2006. Extinction; how Life on Earth Nearly Ended 250 Million Years Ago. Princeton Univ. Press, New Jersey, United States, 296 pp.

Falcon, R.M.S., 1986. Classification of coals in Southern Africa. In: Anhaeusser, C.R., Maske, S. (Eds.), Mineral Deposits of Southern Africa, vols. I and II. Geol. Soc. S, Africa, Johannesburg, pp. 1899–1921.

Falcon, R.M.S., Snyman, C.P., 1986. An introduction to coal petrography: Atlas of Petrographic constituents in the bituminous coals of southern Africa. In: Geol. Soc. S. Afr. Rev (Paper No. 2).

Faure, G., 2001. The Origin of Igneous Rocks; The Isotopic Evidence. Springer, Heidelberg, Germany, 511 pp.

Faure, G., Mensing, T.M., 2010. The Transantarctic Mountains: Rock, Ice, Meteorites and Water. Springer Science + Business Media B.V, 804 pp.

Faure, K., de Wit, M.J., Willis, J.P., 1995. Late Permian global coal hiatus linked to ^{13}C-depleted CO_2 flux into the atmosphere during the final consolidation of Pangea. Geology 23, 507–510.

Fitzgerald, P.G., 1992. The Transantarctic Mountains in southern Victoria Land: the application of apatite fission track analysis to a rift shoulder uplift. Tectonics 11, 634–662.

Fitzgerald, P.G., 1994. Thermochronologic constraints on post-Paleozoic tectonic evolution of the central Transantarctic Mountains, Antarctica. Tectonics 13, 818–836.

Fleming, T.H., Heimann, A., Foland, K.A., Elliott, D.H., 1997. $^{40}Ar/^{39}Ar$ geochronology of Ferrar Dolerite sills from the Transantarctic Mountains, Antarctica: implications for the age and origin of the Ferrar magmatic province. GSA Bull. 109, 533–546.

Fredericks, P.M., Warbrooke, P., Wilson, M.A., 1985. A study of the effect of igneous intrusions on the structure of an Australian high volatile bituminous coal. Org. Geochem. 8, 329–340.

Ganino, C., Arndt, N.T., 2009. Climate changes caused by degassing of sediments during the emplacement of large igneous provinces. Geology 37, 323–326.

Goodarzi, F., Gentizis, T., Jackson, G., MacQueen, R.W., 1993. Optical characteristics of heat-affected bitumens from the Nanisivik Mine, N.W. Baffin Island, Arctic Canada. Energy Sources 15, 359–376.

Goodarzi, F., Gentzis, T., Grasby, S.E., Dewing, K., 2018. Influence of igneous intrusions on thermal maturity and optical texture: comparison between a bituminous marl and a coal seam of the same maturity. Int. J. Coal Geol. 198, 183–197.

Goodarzi, F., Gentzis, T., Dewing, K., 2019. Influence of igneous intrusions on the thermal maturity of organic matter in the Sverdrup Basin, Arctic Canada. Int. J. Coal Geol. 213, 103280.

Grasby, S.E., Beauchamp, B., 2008. Intrabasin variability of the carbon isotope record across the Permian–Triassic transition, Sverdrup basin, arctic Canada. Chem. Geol. 253, 141–150.

Grasby, S.E., Sanei, H., Beauchamp, B., 2011. Catastrophic dispersion of coal fly ash into oceans during the latest Permian extinction. Nat. Geosci. 4, 104–107.

Gröcke, D.R., 1998. Carbon-isotope anlayses of fossil plants as a chemostratigraphic and palaeoenvironmental tool. Lethaia 31, 1–13.
Gröcke, D.R., 2002. The carbon isotope composition of ancient CO_2 based on higher-plant organic matter. Phil. Trans. R. Soc. Lond. A 360, 633–638.
Gröcke, D.R., Rimmer, S.M., Yoksoulian, L.E., Cairncross, B., Tsikos, H., 2009. No evidence for large-scale thermogenic methane release by the Karoo-Ferrar large igneous province. Earth Planet. Sci. Lett. 277, 204–212.
Guo, Y., Bustin, R.M., 1998. FTIR spectroscopy and reflectance of modern charcoals and fungal decayed, woods: implications for studies of inertinites in coals. Int. J. Coal Geol. 37, 29–53.
Gurba, L.W., Weber, C.R., 2001. Effects of igneous intrusions on coal bed methane potential, Gunnedah Basin, Australia. Int. J. Coal Geol. 46, 113–131.
Hallam, A., Wignall, P.B., 1997. Mass Extinctions and their Aftermath. Oxford University Press, 320 pp.
Hansen, H.J., 2006. Stable isotopes of carbon from basaltic rocks and their possible relation to atmospheric isotope excursions. Lithos 92, 105–116.
Hoefs, J., Frey, M., 1976. The isotopic composition of carbonaceous matter in a metamorphic profile from the Swiss Alps. Geochim. Cosmochim. Acta 40, 945–951.
Holdgate, G.R., McLoughlin, S., Drinnan, A.N., Finkelman, R.B., Willett, J.C., Chiehowsky, L.A., 2005. Inorganic chemistry, petrography and paleobotany of Permian coals in the Price Charles Mountains, East Antarctica. Int. J. Coal Geol. 63, 156–177.
Holser, W.T., Schönlaub, H.P., Attrep, M., Boeckelmann, K., Klein, P., Margaritz, M., Orth, C.J., Fenninger, A., Jenny, C., Kralik, M., Mauritsch, H., Pak, E., Schramm, J. M., Stattegger, K., Schmöller, R., 1989. A unique geochemical record at the Permian/Triassic boundary. Nature 337, 39–44.
Holser, W.T., Magaritz, M., Ripperdan, R.L., 1996. Global isotopic events. In: Walliser, O. H. (Ed.), Global Events and Event Stratigraphy in the Phanerozoic. Springer, Berlin and New York, pp. 63–88.
Horacek, M., Brandner, R., Abart, R., 2007a. Carbon isotope record of the P/T boundary and the Lower Triassic in the Southern Alps: evidence for rapid changes in storage of organic carbon. Palaeogeogr. Palaeoclimatol. Palaeoecol. 252, 347–354.
Horacek, M., Richoz, S., Brandner, R., Krystyn, L., Spötl, C., 2007b. Evidence for recurrent changes in Lower Triassic oceanic circulation of the Tethys: the $\delta^{13}C$ record from marine sections in Iran. Palaeogeogr. Palaeoclimatol. Palaeoecol. 252, 355–369.
Horner, T.C., Krissek, L.A., 1991. Contributions of sedimentologic thermal alteration and organic carbon data to paleoenvironmental interpretation of fine-grained Permian clastics from the Beardmore Glacier region, Antarctica. In: Elliot, D.H. (Ed.), Contributions to Antarctic Research, Antarctic Research Series, Amer. Geophys. Union, vol. 53, pp. 33–65.
Hower, J.C., O'Keefe, J.M.K., Watt, M.A., Pratt, T.J., Eble, C.F., Stucker, J.D., Richardson, A.R., Kostova, I.J., 2009. Notes on the origin of inertinite macerals in coals: observations on the importance of fungi in the origin of macrinite. Int. J. Coal Geol. 80, 135–143.
Hower, J.C., O'Keefe, J.M.K., Eble, C.F., Raymond, A., Valentim, B., Volk, T.J., Richardson, A.R., Satterwhite, A.B., Hatch, R.S., Stucker, J.D., Watt, M.A., 2011. Notes on the origin of inertinite macerals in coal: evidence for fungal and arthropod transformations of degraded macerals. Int. J. Coal Geol. 86, 231–240.
Hower, J.C., Misz-Keenan, M., O'Keefe, J.M.K., Mastalerz, M., Eble, C.F., Garrison, T.M., Johnston, M.N., Stucker, J.D., 2013. Macrinite forms in Pennsylvanian coals. Int. J. Coal Geol. 116–117, 172–181.
Hudspith, V., Scott, A.C., Collinson, M.E., Pronina, N., Beeley, T., 2012. Evaluating the extent to which wildfire history can be interpreted from inertinite distribution in coal pillars: an example from the late Permian, Kuznetsk basin, Russia. Int. J. Coal Geol. 89, 13–25.
Jin, Y.G., Wang, Y., Wang, W., Shang, Q.H., Cao, C.Q., Erwin, D.H., 2000. Pattern of marine mass extinction near the Permian–Triassic boundary in South China. Science 289, 432–436.
Jones, T.P., Chaloner, W.G., 1991. Fossil charcoal, its recognition and palaeoatmospheric significance. Palaeogeogr. Palaeoclimatol. Palaeoecol. 97, 39–50.
Jones, J.M., Creaney, S., 1977. Optical character of thermally metamorphosed coals of northern England. J. Microsc. 109, 105–118.
Jüntgen, H., Karweil, J., 1966. Gasbildung und Gasspeicherung in Steinkohlenflozen. I. Gasbildung. Erdol Kohle 19, 251–258.
Kajiwara, Y., Yamakita, S., Ishida, K., Ishiga, H., Imai, A., 1994. Development of a largely anoxic stratified ocean and its temporary massive mixing at the Permian/Triassic boundary supported by the sulfur isotopic record. Palaeogeogr. Palaeoclimatol. Palaeoecol. 111, 367–379.
Kamo, S.L., Czamanske, G.K., Amelin, Y., Fedorenko, V.A., Davis, D.W., Trofimov, V.R., 2003. Rapid eruption of Siberian flood-volcanic rocks and evidence for coincidence with the Permian–Triassic boundary and mass extinction at 251 Ma. Earth Planet. Sci. Lett. 214, 75–91.
Knoll, A.H., Bambach, R.K., Canfield, D.E., Grotzinger, J.P., 1996. Comparative earth history and late Permian mass extinction. Science 273, 452–457.
Kohn, M.J., 2010. Carbon isotope compositions of terrestrial C3 plants as indicators of (paleo) ecology and (paleo) climate. Proc. Natl. Acad. Sci. 107 (46), 19691–19695.
Korte, C., Kozur, H.W., 2010. Carbon-isotope stratigraphy across the Permian–Triassic boundary: a review. J. Asian Earth Sci. 39, 215–235.
Krull, E.S., Retallack, G.J., 2000. $\delta^{13}C$ depth profiles from paleosols across the Permian–Triassic boundary: evidence for methane release. GSA Bull. 112, 1459–1472.
Krull, E.S., Retallack, G.J., Campbell, H.J., Lyon, G.L., 2000. $\delta^{13}C_{org}$ chemostratigraphy of the Permian-Triassic boundary in the Maitai Group, New Zealand: evidence for high-latitudinal methane release. New Zealand J. Geol. Geophys. 43, 21–32.
Krull, E.S., Lehrmann, D.J., Druke, D., Kessel, B., Yu, Y.-Y., Li, R.-X., 2004. Stable carbon isotope stratigraphy across the Permian-Triassic boundary in shallow marine platforms, Nanpanjiang Basin, South China. Palaeogeogr. Palaeoclimatol. Palaeoecol. 204, 297–315.
Kruszewska, K., 2003. Fluorescing macerals in South African coals. Int. J. Coal Geol. 54, 79–94.
Kump, L.R., Arthur, M.A., 1999. Interpreting carbon-isotope excursions: carbonates and organic matter. Chem. Geol. 161, 181–198.
Kwiecińska, B.K., Patersen, H.I., 2004. Graphite, semi-graphite, natural coke, and natural char classification – ICCP system. Int. J. Coal Geol. 57, 99–116.
Kwiecińska, B.K., Pusz, S., 2016. Pyrolytic carbon – Definition, classification and occurrence. Int. J. Coal Geol. 163, 1–7.
Li, K., Rimmer, S.M., Liu, Q., 2018. Geochemical and petrographic analysis of graphitized coals from Central Hunan, China. Int. J. Coal Geol. 195, 267–279.
Lisker, F., Läufer, A.L., 2013. The Mesozoic Victoria Basin: vanished link between Antarctica and Australia. Geology 41 (10), 1043–1046.
Long, W.E., 1962. Sedimentary rocks of the Buckeye Range, Horlick Mountains, Antarctica. Science 136, 319–321.
Long, W.E., 1964. The Stratigraphy of the Ohio Range, Antarctica.. Unpubl. Ph.D. dissertation, Ohio State University, Columbus, OH, 342 pp.
Long, W.E., 1965. Stratigraphy of the Ohio Range, Antarctica. In: Hadley, J.B. (Ed.), Geology and Paleontology of the Antarctic. Antarc. Res. Ser, 6. Amer. Geophys. Union, Washington, DC, pp. 71–116.
Magaritz, M., Bär, R., Baud, A., Holser, W.T., 1988. The carbon-isotope shift at the Permian/Triassic boundary in the Southern Alps is gradual. Nature 331, 337–339.
Mastalerz, M., Schimmelmann, A., 2002. Isotopically exchangeable organic hydrogen in coal relates to thermal maturity and maceral composition. Org. Geochem. 33, 921–931.
Matsuoka, K., Skoglund, A., Roth, G., 2018. Quantarctica [Data Set]. Norwegian Polar Institute. https://doi.org/10.21334/npolar.2018.8516e961.
Matsuoka, K., Skogland, A., Roth, G., de Pomereu, J., Griffiths, H., Headland, R., Herried, B., Katsumata, K., Le Brocq, A., Licht, K., Morgan, F., Neff, P.D., Ritz, C., Scheinert, M., Tamura, T., Van de Putte, A., van den Broeke, M., von Deschwanden, A., Deschamps-Berger, C., Van Liefferinge, B., Tronstand, S., Melvær, Y., 2021. Quantarctica, an integrated mapping environment for Antarctica, the Southern Ocean, and sub-Antarctic islands. Environ. Model. Softw. 140, 105015.
McElwain, J., Wade-Murphy, J., Hesselbo, S.P., 2005. Changes in carbon dioxide during an oceanic anoxic event linked to intrusion into Gondwana coals. Nature 435, 479–482.
McKirdy, D.M., Powell, T.G., 1974. Metamorphic alteration of carbon isotopic composition in ancient sedimentary organic matter. New evidence from Australia and South Africa. Geology 2, 591–595.
Meyers, P.A., Simoneit, B.R.T., 1999. Effects of extreme heating on the elemental and isotopic compositions of an Upper Cretaceous coal. Org. Geochem. 30, 299–305.
Minshew, V.H., 1966. Stratigraphy of the Wisconsin Range, Horlick Mountains, Antarctica. Science 152, 637–638.
Morante, R., 1996. Permian and Early Triassic isotopic records of carbon and strontium in Australia and a scenario of events about the Permian-Triassic boundary. Hist. Biol. 11, 289–310.
Moroeng, O.M., Wagner, N.J., Hall, G., Roberts, R.J., 2018. Using $d^{15}N$ and $d^{13}C$ and nitrogen functionalities to support a fire origin for certain inertinite macerals in a No. 4 Seam Upper Witbank coal, South Africa. Org. Geochem. 126, 23–32.
Murchison, D., 2004. Aberrations in the coalification patterns of the offshore coalfields of Northumberland and Durham, United Kingdom. Int. J. Coal Geol. 58, 133–146.
Murchison, D., 2006. The influence of heating rate on organic matter in laboratory and natural environments. Int. J. Coal Geol. 67, 145–157.
Pálfy, J., Smith, P.L., 2000. Synchrony between Early Jurassic extinction, oceanic anoxic event, and the Karoo–Ferrar flood basalt volcanism. Geology 28, 747–750.
Pearson, D., Murchison, D., 1999. Relationship between reflectance and volatile-matter yield at the Maudlin (H) horizon of the offshore Northumberland and Durham coalfields. Fuel 78, 1417–1423.
Perregaard, J., Scheiner, E.J., 1979. Thermal alteration of sedimentary organic matter by a basalt intrusive (Kimmeridgian Shales, Milne Land, East Greenland). Chem. Geol. 26, 331–343.
Petsch, S.T., Edwards, K.J., Eglinton, T.I., 2003. Abundance, distribution and $\delta^{13}C$ analysis of microbial phospholipid-derived fatty acids in a black shale weathering profile. Org. Geochem. 34, 731–743.
Polozov, A.G., Svensen, H.H., Planke, S., Grishina, S.N., Fristad, K.E., Jerram, D.A., 2016. The basalt pipes of the Tunguska Basin (Siberia, Russia): high temperature processes and volatile degassing into the end-Permian atmosphere. Palaeogeogr. Palaeoclimatol. Palaeoecol. 441, 51–64.
Presswood, S.M., Rimmer, S.M., Anderson, K.B., Filiberto, J., 2016. Geochemical and petrographic alteration of rapidly heated coals from the Herrin (No. 6) coal Seam, Illinois Basin. Int. J. Coal Geol. 165, 243–256.
Quaderer, A., Mastalerz, M., Schimmelmanss, A., Drobniak, A., Bish, D.L., Wintsch, R.P., 2016. Dike-induced thermal alteration of the Springfield Coal Member (Pennsylvanian) and adjacent clastic rocks, Illinois Basin, USA. Int. J. Coal Geol. 166, 108–117.
Rahman, M.W., Rimmer, S.M., 2014. Effects of rapid thermal alteration on coal: geochemical and petrographic signatures in the Springfield (No. 5) coal, Illinois Basin. Int. J. Coal Geol. 131, 214–226.
Rahman, M.W., Rimmer, S.M., Rowe, H.D., Huggett, W.W., 2017. Carbon isotope analysis of whole-coal samples and vitrinite fractions from intruded coals from the Illinois Basin: no isotopic evidence for thermogenic methane generation. Chem. Geol. 453, 1–11.

Rampino, M.R., Strothers, R.B., 1988. Flood basalt volcanism during the last 250 million years. Science 241, 663–667.
Rampino, M.R., Rodriguez, S., Baransky, E., Cai, Y., 2017. Global nickel anomaly links Siberian Traps eruptions and the latest Permian mass extinction. Sci. Rep. 7, 12416.
Raup, D.M., Sepkoski, J.J., 1982. Mass extinction in the marine record. Science 215, 1501–1503.
Raymond, A.C., Murchison, D.G., 1988. Development of organic maturation in the thermal aureoles of sills and its relation to sediment compaction. Fuel 67, 1599–1608.
Reichow, M.K., Pringle, M.S., Al'Mukhamedov, A.I., Allen, M.B., Andreichev, V.I., Buslov, M.M., Davies, C.E., Fedoseev, G.S., Fitton, J.G., Inger, S., Medvedev, A. Ya, Mitchell, C., Puchkov, V.N., Safonova Yu, I., Scott, R.A., Saunders, A.D., 2009. The timing and extent of the eruption of the Siberian Traps large igneous province: Implications for the end-Permian environmental crisis. Earth Planet. Sci. Lett. 277, 9–20.
Renne, P.R., Basu, A.R., 1991. Rapid eruption of the Siberian traps flood basalts at the Permian-Triassic boundary. Science 253, 176–179.
Renne, P.R., Zichao, Z., Richards, M.A., Black, M., Basu, A.R., 1995. Synchrony and causal relations between Permian-Triassic boundary crises and Siberian flood volcanism. Science 269, 1413–1416.
Retallack, G.J., 1995. Permian-Triassic life crisis on land. Science 267, 77–80.
Retallack, G.J., Greaver, T., 2007. Return to Coalsack Bluff and the Permian-Triassic boundary in Antarctica. Glob. Planet. Chang. 55, 90–108.
Retallack, G.J., Jahren, A.H., 2008. Methane release from igneous intrusion of coal during Late Permian extinction events. J. Geol. 116, 1–20.
Retallack, G.J., Krull, E.S., 1999. Landscape ecological shift at the Permian-Triassic boundary in Antarctica. Austr. J. Earth Sci. 46, 786–812.
Retallack, G.J., Metzger, C.A., Greaver, T., Jahren, A.H., Smith, R.M.H., Sheldon, N.D., 2006. Middle-Late Permian mass extinction on land. GSA Bull. 118, 1398–1411.
Richoz, S., 2006. Stratigraphie et variations isotopiques du carbone dans le Permien supérieur et le Trias inférieur de la Néotéthys (Turquie, Oman et Iran). Mem. Géol. 46, 251.
Rimmer, S.M., Rowe, H.D., Taulbee, D.N., Hower, J.C., 2006. Influence of maceral content on $\delta^{13}C$ and $\delta^{15}N$ in a Middle Pennsylvanian coal. Chem. Geol. 225, 77–90.
Rimmer, S.M., Yoksoulian, L.E., Hower, J.C., 2009. Anatomy of an intruded coal, I: effect of contact metamorphism on whole-coal geochemistry, Springfield (No. 5) (Pennsylvanian) coal, Illinois Basin. Int. J. Coal Geol. 79, 74–82.
Robinson, S.A., Hesselbo, S.P., 2004. Fossil–wood carbon-isotope stratigraphy of the non-marine Wealden Group (Lower Cretaceous, southern England). J. Geol. Soc. Lond. 161, 133–145.
Rothman, D.H., Fournier, G.P., French, K.L., Alm, E.J., Boyle, E.A., Cao, C., Summons, R. E., 2014. Methanogenic burst in the end-Permian carbon cycle. Proc. Natl. Acad. Sci. U. S. A. 111, 5462–5467.
Ryskin, G., 2003. Methane-driven oceanic eruptions and mass extinctions. Geology 31, 741–744.
Sackett, W.M., 1978. Carbon and hydrogen isotope effects during the thermocatalytic production of hydrocarbons in laboratory simulation experiments. Geochim. Cosmochim. Acta 42, 571–580.
Saghafi, A., Pinetown, K.L., Grobler, P.G., van Heerden, J.H.P., 2008. CO_2 storage potential of South African coals and gas entrapment enhancement due to igneous intrusions. Int. J. Coal Geol. 73, 74–87.
Saitoh, M., Isozaki, Y., 2021. Carbon isotope chemostratigraphy across the Permian-Triassic boundary at Chaotian, China: implications for the global methane cycle in the aftermath of the extinction. Front. Earth Sci. 8, 596178.
Sanders, M.M., 2012. Geochemistry and Petrography of Thermally Metamorphosed Antarctic Coal: Implications for ^{13}C-depleted Methane Release.. Unpubl. M.S. Thesis, Southern Illinois University Carbondale, Carbondale IL, 113 pp.
Sanders, M.M., Rimmer, S.M., 2020. Revisiting the thermally metamorphosed coals of the Transantarctic Mountains, Antarctica. Int. J. Coal Geol. 228, 103550.
Sarkar, A., Yoshioka, H., Ebihara, M., Naraoka, H., 2003. Geochemical and organic carbon isotope studies across the continental Permo–Triassic boundary of Raniganj Basin, eastern India. Palaeogeogr. Palaeoclimatol. Palaeoecol. 191, 1–14.
Saxby, J.D., Stephenson, L.C., 1987. Effect of an igneous intrusion on oil shale at Rundle (Australia). Chem. Geol. 63, 1–16.
Schapiro, N., Gray, R.J., 1966. Physical variations in highly metamorphosed Antarctic coals. In: Gould, R.F. (Ed.), Coal Science, 55. Amer. Chem. Soc., Adv. Chem. Ser, pp. 196–210.
Schimmelmann, A., Mastalerz, M., Ling, G., Sauer, P., Topalov, K., 2009. Dike intrusions into bituminous coal: H, C, N, O isotopic responses to rapid and brief heating. Geochim. Cosmochim. Acta 73, 6264–6281.
Schneebeli-Hermann, E., Kürschner, W.M., Hochuli, P.A., Ware, D., Weissert, H., Bernasconi, S.M., Roohi, R., Ur-Rehman, K., Goudemand, N., Bucher, H., 2013. Evidence for atmospheric carbon injection during the end-Permian extinction. Geology 41, 579–582.
Schobben, M., Ullmann, C.V., Leda, L., Korn, D., Struck, U., Reimold, W.U., Ghaderi, A., Algeo, T.J., Korte, C., 2016. Discerning primary versus diagenetic signals in carbonate carbon and oxygen isotope records: an example from the Permian–Triassic boundary of Iran. Chem. Geol. 422, 94–107.
Scholze, F., Wang, X., Kirscher, U., Kraft, J., Schneider, J.W., Götz, A.E., Joachimski, M. M., Bachtadse, V., 2017. A multistratigraphic approach to pinpoint the Permian-Triassic boundary in continental deposits: the Zechstein–Lower Buntsandstein transition in Germany. Glob. Planet. Chang. 152, 129–151.
Schopf, J.M., 1962. A preliminary report on plant remains and coal of the sedimentary section in the central Horlick Mountains, Antarctica. In: Inst. of Polar Studies Rept, 2. The Ohio State University, Columbus, OH, 62 pp.
Schopf, J.M., Long, W.E., 1966. Coal metamorphism and igneous associations in Antarctica. In: Gould, R.F. (Ed.), Coal Science, 55. Amer. Chem. Soc., Adv. Chem. Ser, pp. 156–195.
Schubert, B.A., Jahren, A.H., 2012. The effect of atmospheric CO_2 concentration on carbon isotope fractionation in C_3 land plants. Geochim. Cosmochim. Acta 96, 29–43.
Scott, A.C., Glasspool, I.J., 2007. Observations and experiments on the origin and formation of inertinite group macerals. Int. J. Coal Geol. 70, 53–66.
Sephton, M.A., Looy, C.V., Brinkhuis, H., Wignall, P.B., de Leeuw, J.W., Visscher, H., 2005. Catastrophic soil erosion during the end-Permian biotic crisis. Geology. 33, 941–944.
Shen, S.Z., Crowley, J.L., Wang, Y., Bowring, S.A., Erwin, D.H., Sadler, P.M., Cao, C.Q., Rothman, D.H., Henderson, C.M., Ramezani, J., Zhan, H., Shen, Y., Wang, X.D., Wang, W., Mu, L., Li, W.Z., Tang, Y.G., Liu, X.L., Liu, L.J., Zeng, Y., Jian, Y.F., Jin, Y. G., 2011. Calibrating the end-Permian mass extinction. Science 334, 1367–1372.
Shen, J., Algeo, T.J., Hu, Q., Zhang, N., Zhou, L., Xia, W., Xie, S., Feng, Q., 2012. Negative C-isotope excursions at the Permian-Triassic boundary linked to volcanism. Geology 40, 963–966.
Shen, S.Z., Cao, C.Q., Zhang, H., Bowring, S.A., Henderson, C.M., Payne, J.L., Davydov, V.I., Chen, B., Yuan, D., Zhang, Y., Wang, W., Zheng, Q., 2013. High-resolution $\delta^{13}C_{carb}$ chemostratigraphy from latest Guadalupian through earliest Triassic in South China and Iran. Earth Planet. Sci. Lett. 375, 156–165.
Slater, L.E., 2009. The Petrography of Ancient Organic Matter in Kerogen Weathering Profiles.. Unpublished M.S. thesis, University of Kentucky, Lexington, KY, 90 pp.
Snyman, C.P., Botha, W.J., 1993. Coal in South Africa. J. Afr. Earth Sci. 15, 171–180.
Stanley, S.M., 2016. Estimates of the magnitudes of major marine mass extinctions in earth history. Proc. Natl. Acad. Sci. U. S. A. 113, E6325–E6334.
Stewart, A.K., Massey, M., Padgett, P.L., Rimmer, S.M., Hower, J.C., 2005. Influence of basic intrusion on the vitrinite reflectance and chemistry of the Springfield (No. 5) coal, Harrisburg, Illinois. Int. J. Coal Geol. 63, 58–67.
Storm, M.S., Hesselbo, S.P., Jenkyns, H.C., Ruhl, M., Ullmann, C.V., Xu, W., Leng, M.J., Riding, J.B., Gorbanenko, O., 2022. Orbital pacing and secular evolution of the Early Jurassic carbon cycle. Proc. Natl. Acad. Sci. U. S. A. 117, 3974–3982.
Svensen, H., Planke, S., Chevallier, L., Malthe-Sørenssen, A., Corfu, F., Jamtveit, B., 2004. Hydrothermal venting of greenhouse gases triggering Early Jurassic global warming. Earth Planet. Sci. Lett. 256, 554–566.
Svensen, H., Planke, S., Malthe-Sørenssen, A., Jamtveit, B., Myklebust, R., Rasmussen, E., Torfinn, R., Rey, S.S., 2007. Release of methane from a volcanic basin as a mechanism for initial Eocene global warming. Nature 429, 542–545.
Svensen, H., Planke, S., Polozov, A.G., Schmidbauer, N., Corfu, F., Podladchikov, Y.Y., Jamtveit, B., 2009. Siberian gas venting and the end-Permian environmental crisis. Earth Planet. Sci. Lett. 277, 490–500.
Takahashi, S., Kaiho, K., Oba, M., Kakegawa, T., 2010. A smooth negative shift of organic carbon isotope ratios at an end-Permian mass extinction horizon in central pelagic Panthalassa. Palaeogeogr. Palaeoclimatol. Palaeoecol. 292, 532–539.
Taylor, G.H., 1961. Development of optical properties of coke during carbonization. Fuel 40, 465–472.
Taylor, G.H., Teichmüller, M., Davis, A., Diessel, C.F.K., Littke, R., Robert, P., 1998. Organic Petrology. Gebrüder Borntraeger, Berlin, 704 pp.
Twitchett, R.J., Looy, C.V., Morante, R., Visscher, H., Wignall, P.B., 2001. Rapid and synchronous collapse of marine and terrestrial ecosystems during the end-Permian biotic crisis. Geology 29, 351–354.
van de Schootbrugge, B., Payne, J.L., Tomasovych, A., Pross, J., Fiebig, J., Benbrahim, M., Föllmi, K.B., Quan, T.M., 2008. Carbon cycle perturbation and stabilization in the wake of the Triassic–Jurassic boundary mass-extinction event. Geochem. Geophys. Geosyst. 9, Q04028.
Van de Wetering, N., Esterle, J.S., Golding, S.D., Rodrigues, S., Götz, A.E., 2019. Carbon isotoptic evidence for rapid methane clathrate release recorded in coals at the terminus of the Late Paleozoic Ice Age. Nat. Sci. Rep. 9, 16544.
van Krevelen, D.W., Schuyer, J., 1957. Coal Science: Aspects of Coal Constitution. Elsevier, Amsterdam, p. 352.
Wagner, N., Eble, C., Hower, J.C., Falcon, R., 2019. Petrology and palynology of select coal samples from the Permian Waterberg Coalfield, South Africa. Int. J. Coal Geol. 204, 85–101.
Ward, P.D., Montgomery, D.R., Smith, R., 2000. Altered river morphology in South Africa related to the Permian–Triassic extinction. Science 289, 1740–1743.
Whiticar, M.J., 1996. Stable isotope geochemistry of coals, humic kerogens and related natural gases. Int. J. Coal Geol. 32, 191–215.
Wignall, P.B., 2001. Large igneous provinces and mass extinctions. Earth-Sci. Rev. 53, 1–33.
Wignall, P.B., Morante, R., Newton, R., 1998. The Permo–Triassic transition in Spitsbergen: $\delta^{13}C_{org}$ chemostratigraphy, Fe and S geochemistry, facies, fauna and trace fossils. Geol. Mag. 135, 47–62.
Wu, Y., Chu, D., Tong, J., Song, H., Dal Corso, J., Wignall, P.B., Song, H., Du, Y., Cui, Y., 2021. Six-fold increase of atmospheric pCO_2 during the Permian–Triassic mass extinction. Nat. Commun. 12, 2137.
Xu, D.-Y., Yan, Z., 1993. Carbon isotope and iridium event markers near the Permian/Triassic boundary in the Meishan section, Zhejiang Province, China. Paleogeogr. Palaeoclimat. Paleoecol. 104, 171–176.
Yin, H., Sweet, W.C., Glenister, B.F., Kotlyar, G., Kozur, H., Newell, N.D., Sheng, J.Y., Zakharov, Y.D., 1996. Recommendations of the Meishan section as global stratotype section and point for basal boundary of Triassic system. Newsl. Stratigr. 34, 81–108.

Yoksoulian, L.E., 2010. Effect of Contact Metamorphism on Coal Geochemistry and Petrology: Implications for the Large-Scale Release of ^{12}C-enriched Methane.. Unpubl. Ph.D. Dissertation, University of Kentucky, Lexington, KY, 133 pp.

Yoksoulian, L.E., Rimmer, S.M., Rowe, H.D., 2016. Anatomy of an intruded coal, II: effect of contact metamorphism on organic δ^{13}C and implications for the release of thermogenic methane, Springfield (No. 5) coal, Illinois Basin. Int. J. Coal Geol. 158, 129–136.

Zuchuat, V., Sleveland, A.R.N., Twitchett, R.J., Svensen, H.H., Turner, H., Augland, L.E., Jones, M.T., Hammer, Ø., Hauksson, B.T., Haflidason, H., Midtkandal, I., Planke, S., 2020. A new high-resolution stratigraphic and palaeoenvironmental record spanning the End-Permian Mass Extinction and its aftermath in Central Spitsbergen. Svalbard. Palaeogeogr. Palaeoclimatol. Palaeoecol. 554, 109732.